1995

High-Resolution Seismic Stratigraphy of the Ganges-Brahmaputra River System: Subaqueous Deltaic Progradation on the Bengal Shelf

Beth Michele Levy
College of William and Mary - Virginia Institute of Marine Science

HIGH-RESOLUTION SEISMIC STRATIGRAPHY OF THE GANGES-BRAHMAPUTRA RIVER SYSTEM: SUBAQUEOUS DELTAIC PROGRADATION ON THE BENGAL SHELF

A Thesis
Presented to
The Faculty of the School of Marine Science
The College of William and Mary in Virginia

In partial Fulfillment
Of the Requirements for the Degree
Master of Arts

---

by
Beth Michele Levy
1995

This thesis is submitted in partial fulfillment
of the requirements for the degree of

Master of Arts

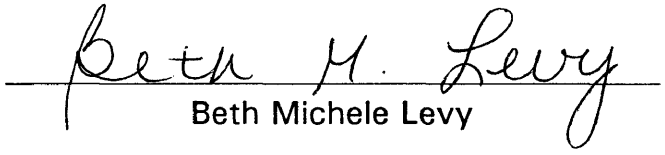

Beth Michele Levy

Approved July 1995

Steven A. Kuehl, Ph.D.
Committee Chairman/Advisor

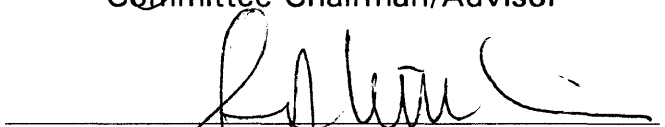

John D. Milliman, Ph.D.

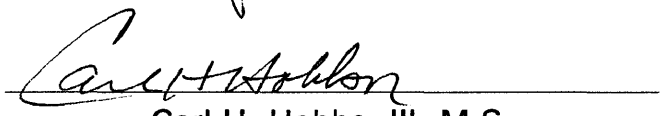

Carl H. Hobbs, III, M.S.

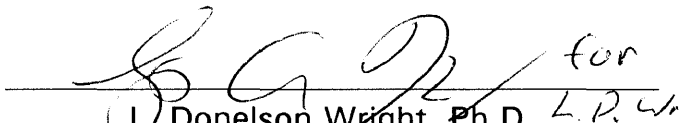

L. Donelson Wright, Ph.D. for L. D. Wright

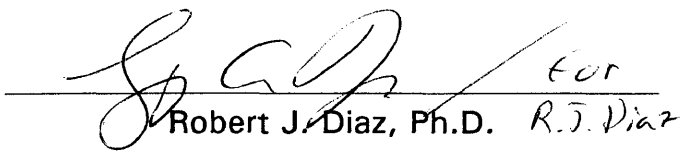

Robert J. Diaz, Ph.D. for R. J. Diaz

SUBAQUEOUS DELTAIC PROGRADATION ON THE BENGAL SHELF

TABLE OF CONTENTS

Page

ACKNOWLEDGEMENTS

I would like to thanks my major advisor, Steve Kuehl, for all his help and guidance throughout this research. I would also like to thank my committee for their input and support. The encouragement, and (mostly) good natured harassment of Tim Dellapenna and Steve Goodbred is gratefully acknowledged.

Completion of this project, as well as my mental stability, would not have been possible without the support of my friends and family who assured me, adnauseam, that my IQ is indeed higher than my grade point average and everything would work out, I will never doubt them again.

LIST OF TABLES

LIST OF FIGURES

Abstract

The Ganges-Brahmaputra river system is among the world's largest in terms of sediment load but, until now, no seismic data had been obtained to document the nature of the sediment deposit seaward of the rivers mouths. Other large rivers which likewise discharge into energetic environments (e.g., Amazon, Huanghe) are forming subaqueous deltas with characteristic clinoform stratigraphy. High-resolution seismic reflection profiles of the Bengal shelf, seaward of the Ganges-Brahmaputra, reveal similar clinoform stratigraphy: topset beds dip gently (0.04°) and diverge offshore; more steeply dipping foreset beds (0.19°) converge farther seaward; relatively thin, gently dipping bottomset beds (0.02°) extend across the outer shelf, overlying an erosional surface presumed to be of Late Pleistocene age. Sediment accumulation rates corroborate the relative thickening and thinning of strata in the topset (~1 cm/y), foreset (~10 cm/y) and bottomset (<1 cm/y) areas. Taken together, these data indicate the subaqueous delta is an actively prograding feature. Volume estimates for the Holocene subaqueous delta reveal that about a third of the total load of the present-day Ganges-Brahmaputra accumulates on the shelf. The remainder is likely partitioned between the river flood plain/lower delta plain and off-shelf transport via the submarine canyon, "Swatch of No Ground." The canyon incises the shelf in the area of highest sedimentation rates (foreset), suggesting significant off-shelf transport of sediments to the Bengal Fan. Observations of growth faults and slumping of modern sediments near the head of the canyon further supports this idea. Detailed study of flood plain/lower delta plain sedimentation is needed to assess their relative importance in the overall sediment budget. The characteristics seen in the modern systems are also recognized in the rock record. Both modern and ancient deltas display distinctive clinoform stratigraphy as well as similar distributions of accumulation rates, and small scale structures, suggesting subaqueous deltaic progradation is an important mode of delta growth.

Introduction

Modern river deltas have a range of characteristic morphologies that, to a first approximation, are controlled by the river, tidal, and wave characteristics (Wright and Coleman, 1973). Deltas with extensive subaerial expression, such as the Mississippi delta, commonly are found in quiescent seas, or quiescent locations such as fjords and embayments (Nittrouer et al., 1986). Large rivers entering energetic marine environments display various morphologies. The Columbia River displays no subaerial delta, rather, accumulation occurs as a mid-shelf mud deposit. Rivers with sedimentary loads comparable to the Ganges-Brahmaputra, such as the Amazon and Huanghe Rivers, exhibit predominant or partial subaqueous growth of their deltas (Nittrouer et al., 1986; Prior et al., 1986). Even though the sediment discharge of the Amazon is sufficient to produce a major sedimentary feature (clinoform) on the shelf, large shear stresses appear to prevent or limit significant subaerial growth (Nittrouer et al., 1986).

Although the combined sediment discharge of the Ganges-Brahmaputra River system is among the largest in the world, no significant subaerial progradation of the delta has occurred in the last 200 years (Coleman, 1969).

The Ganges-Brahmaputra, like the Amazon and Huanghe, enters an energetic marine setting. The Bengal shelf seaward of this river system exhibits clinoform-like morphology, however, no seismic data has previously been collected to document characteristic topset, foreset and bottomset stratification (Kuehl et al., 1989). An oceanographic cruise on the Bengal shelf conducted in 1991 obtained bottom samples and the first high-resolution seismic reflection data from this area (Fig. 1). Radioisotope profiles of sediment cores are used to provide rates of modern sediment accumulation on the shelf. Utilizing this unique data set, the main objective of this thesis is to test the idea that a subaqueous delta is presently forming on the Bengal Shelf, and if one is forming, attempt to quantify the rate of deposition. The results of this investigation also will be compared with other large rivers (Amazon, Huanghe), as well as ancient analogues from the interior of the western United States (Cody Shale, Tropic Shale and Tunuk Member of the Mancos Shale) in light of the relatively new understanding of subaqueous deltas as an important mode of deltaic progradation in energetic marine settings.

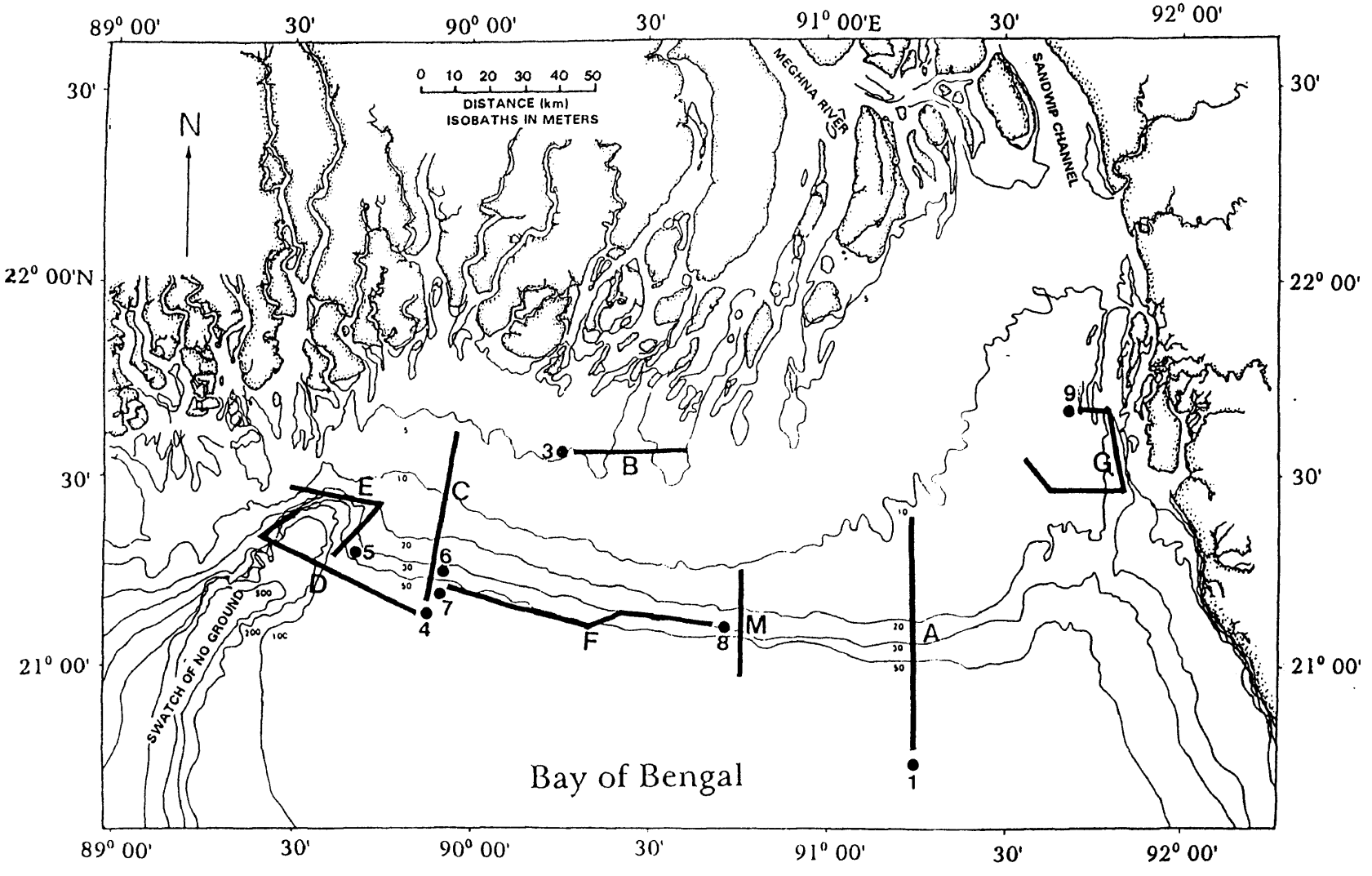

Figure 1 - Bathymetric chart of the Bengal shelf showing station locations (numbers) and seismic transacts (letters).

Background

Subaqueous Deltas

Where there is potential for delta formation, the large-scale morphology is affected by fluvial and oceanographic factors. The amount and grain size of sediments affect the estuarine infilling and progradation of the sediment wedge. Surface waves, tides and currents will further control sediment dispersal and configuration of the resulting stratigraphy (Wright and Coleman, 1973). Seaward of the mouths of the Amazon and Huanghe, subaqueous deltas are forming. These deltas have relief of 10 to 40 m above the adjacent sea floor and display characteristic topset, foreset and bottomset stratigraphy. Nittrouer et al. (1986) believe that subaqueous deltas represent the typical mode of delta formation for large rivers entering dynamic marine environments. Strong tidal currents and surface waves resuspended sediment which is dispersed to less energetic, deeper areas (Kuehl et al., 1986). Rates of sedimentation typically are negligible near shore and increase toward the seaward edge of the topset beds resulting in the seaward divergence of seabed acoustic reflectors in this region. Reflectors in the foreset region converge seaward as a result of a decrease in sedimentation rate. Sedimentation rates in the bottomset region are relatively low, and thin

acoustically transparent beds are common. Because of low accumulation rates on the inner topset beds relative to the foreset beds, the topset region remains subaqueous as the delta progrades (Kuehl, et al., 1986; Alexander, et al., 1991).

Similar stratigraphic relationships are commonly recognized in the geologic record (Fig. 2). Ancient marine shales of the North American Cretaceous such as the Lower Cody Shale of Big Horn Basin in Wyoming (Asquith, 1970), and the Tropic Shale and Tunuk Member of the Mancos Shale in southern Utah (Leithold, 1993) are similar to deposits now forming seaward of the Amazon and Huanghe (Nittrouer et al., 1986; Prior et al., 1986; Bornhold et al, 1986).

Use of Radioisotopes as Geochronometers

The time scale over which radioisotopes are useful is generally 4 to 5 times their half-life. Sediment geochronology based on ^{210}Pb ($t_{1/2}$=22 years), a member of the ^{238}U decay series, allows for the determination of sediment accumulation rates over approximately a 100-year time scale (Koide et al., 1972). ^{210}Pb is supplied from several sources, including offshore coastal waters, riverine input, in situ decay of ^{226}Ra, and precipitation from the atmosphere (DeMaster, et al., 1986). Rapid removal of ^{210}Pb from the water column through scavenging by

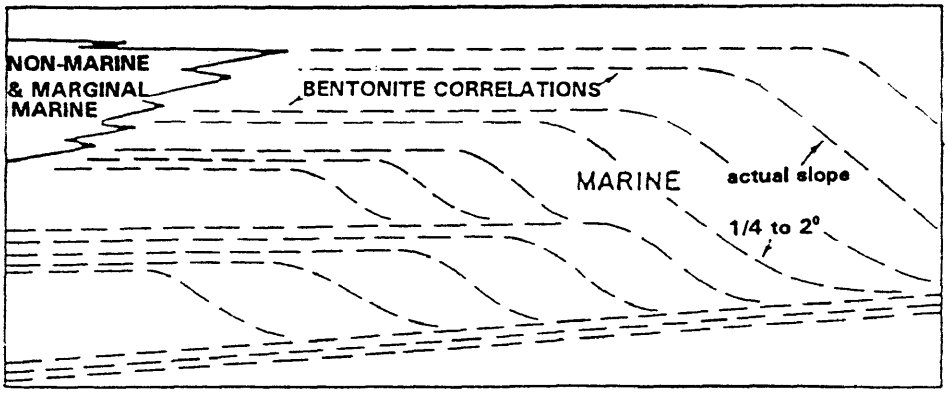

Figure 2 - Cretaceous shale of the interior of the western U.S. (Pierre Shale) displaying characteristic clinoform stratification (from Asquith, 1970).

organisms, adsorption onto particles and co-precipitation with Fe-Mn oxides (DeMaster et al., 1986; McKee et al., 1986) results in activities in excess of ^{226}Ra-supported levels in the seabed. Decay of this excess activity with time (depth) allows for the calculation of sediment accumulation rates. Accumulation rates calculated using ^{210}Pb activities alone typically are considered maximum rates, since the effects of mixing, whether biological or mechanical, cannot be determined.

^{137}Cs is a bomb-produced radioisotope present in the atmosphere since about 1956, and can be used to estimate accumulation rates based on the depth at which ^{137}Cs first appears. This approach also provides maximum accumulation rates because, used alone, the effect of deep mixing cannot be evaluated. However, used in conjunction with ^{210}Pb, ^{137}Cs can provide information on the presence of deep mixing in the seabed. If the maximum penetration depth of ^{137}Cs is deeper than would be estimated from ^{210}Pb alone, mixing has affected the profile and ^{210}Pb accumulation rate is considered an upper limit (Nittrouer et al., 1979).

^{228}Ra/^{226}Ra geochronology has been used by Dukat and Kuehl (in press) in areas of non-steady-state specific initial ^{210}Pb activities on the Amazon continental shelf. The half life of ^{228}Ra ($t_{1/2}$=5.8 years) makes it particularly useful

for time scales of about 30 years. Unlike ^{210}Pb, radium is not strongly particle reactive, but will desorb as a function of the ionic strength of sea water. Desorption of radium from river sediments occurs as the river water mixes with sea water, and approximately 38% of both ^{228}Ra and ^{226}Ra ($t_{1/2}$=1600 years) activities are lost from the suspended sedimentary particles through ionic exchange (Key et al., 1985). This desorption causes a deficit in the activities of the radium isotopes with respect to their parents in recent sediments. With time and burial in the sea bed, the radium isotopes will in grow to secular equilibrium and can be used as geochronometers.

Study Area

Geologic History and Development of the Bengal Fan

The Tethys Sea closed as India moved toward Eurasia, beginning about 53 Ma, subsequently colliding with Asia to form the Himalayas, the world's highest mountain chain (Curray et al., 1982; Klootwijk, 1992). During the Oligocene and Miocene (36-5 Ma) the Himalayas had presumably not been uplifted to the present extent; however, early sections of the modern Bengal Fan are most likely derived from these ancestral Himalayan Mountains (Curray and Moore, 1974).

Erosion and transport of sediments from the Himalayas began filling the newly-formed Bengal Geosyncline, which includes the Bengal Basin, the Bay of Bengal and adjacent areas (Curray et al., 1982). The Bay of Bengal contains the Bengal Fan (Fig. 3), the world's largest submarine fan, which covers an area of nearly 3×10^6 km^2 and exceeds 12 km in thickness (Curray and Moore, 1971; Curray and Emmel, 1982; Emmel and Curray, 1984). The Bengal Fan is separated from its eastern lobe, the Nicobar Fan, by the Ninety East Ridge, one of the most prominent features in the Bay aside from the Fan itself (Curray et al., 1982). The Eastern margin of the fan terminates abruptly at the Andeman-Java Trench.

The submarine canyon, the "Swatch of No Ground," incises the Bengal shelf, extending nearly to the modern shoreline. During Pleistocene lowered sea-levels the canyon presumably channeled virtually all the sediments of the Ganges-Brahmaputra River to the Bengal Fan (Umistu, 1990). Other rivers also supplied sediment to the Fan, including the Krishna, Godavari and Mahanadi rivers, which drain peninsular India; however, the relatively small loads of these flanking sediment sources had little effect on the fan (Curray et al., 1982).

The movement of sediment and the surface topography of the fan are controlled by a complex system of turbidity current channels, most of which

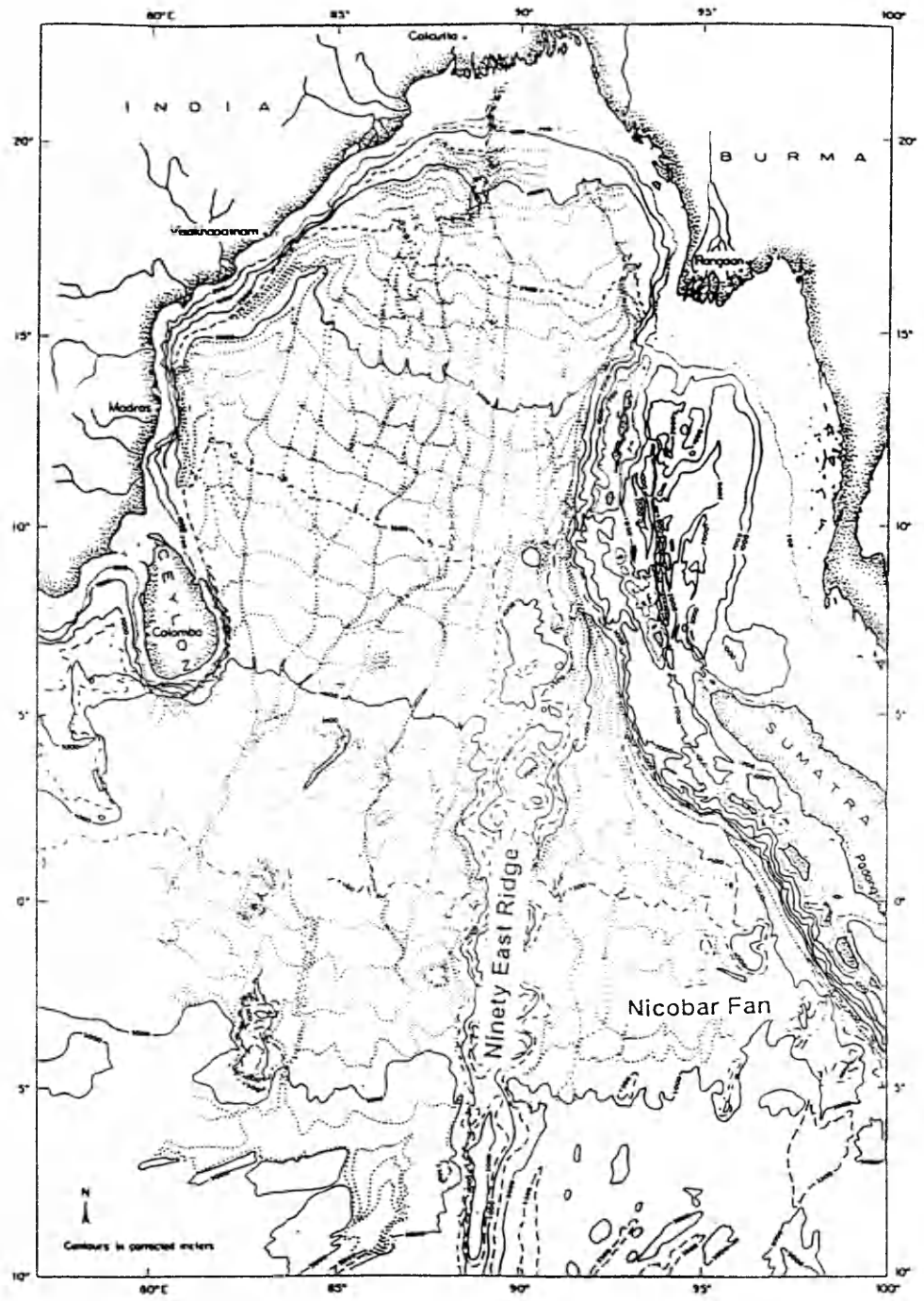

Figure 3 - Bathymetric chart of the Bay of Bengal (from Emmel and Curray, 1985).

originate at the Swatch of No Ground (Curray and Moore, 1971). Large fan valleys sit atop ridges formed of natural levee deposits from the channels. Periodically, these valleys are abandoned and replaced by newly developed valleys on either flank. Curray and Moore (1971) divided the Bengal Fan into the following four stratigraphic units. 1.) *(Quaternary)* The uppermost, and youngest sediments of the modern Bengal Fan which represent turbidite deposition during the most recent era of growth. 2.) *(Late Miocene-Pliocene)* Underlying unit 1 are deformed, folded and locally faulted sediments exposed in outcrops in the southern portion of the Fan and on the Ninety East ridge, primarily produced by turbidity currents. 3.) *(Tertiary)* Older sedimentary rocks and basement rocks, likely of volcanic origin, underlie units 1 and 2 and appear locally as hills. 4.) Acoustical basement rock at the base.

River and Flood Plain Characteristics

The Ganges, Brahmaputra and Meghna Rivers have occupied and abandoned numerous river courses during the Quaternary and have deposited a large, flat, low-lying alluvial plain (Coleman, 1969). This delta plain encompass most of the country of Bangladesh, whose sediments are primarily derived from the erosion of the Himalayas. The Ganges drains much of the south slopes of the

mountains, whereas the Brahmaputra mostly drains the north slopes (Curray and Moore, 1971). The Meghna River drains the northeast part of Bangladesh. The confluence of the Ganges and Brahmaputra rivers occurs about 150 km north of the Bay of Bengal, and the Meghna joins them about 30 km further down stream.

For the delta plain, as well as the Bengal Fan, the Ganges and Brahmaputra rivers are the main source of sediment. The estimated loads of the Ganges and Brahmaputra rivers are 520 x 10^6 t/y and 540 x 10^6 t/y, respectively (Milliman and Syvitski, 1992). The Meghna, in contrast, has a negligible impact on the combined load of the system, contributing only about 1% of the total sediment discharge (Coleman, 1969). Combined sediment transport increases in April-May, peaks in August, and decreases to base level (an order of magnitude less than peak rates) in November (Fig. 4).

Clay-sized mineralogy of Ganges sediment is dominated by smectite (56%) and illite (32%), with minor amounts of chlorite (7%) and kaolinite (5%) (Sarin et al., 1989). In contrast, Brahmaputra sediment is comprised primarily of illite (62%), with lesser amounts of smectite (15%), kaolinite (12%) and chlorite (1%) (Sarin et al., 1989). Even though both rivers drain high-grade metamorphics and acid intrusives, the Ganges also drains Mesozoic basalt traps which explains the higher amount of smectite as opposed to illite (Fig. 5).

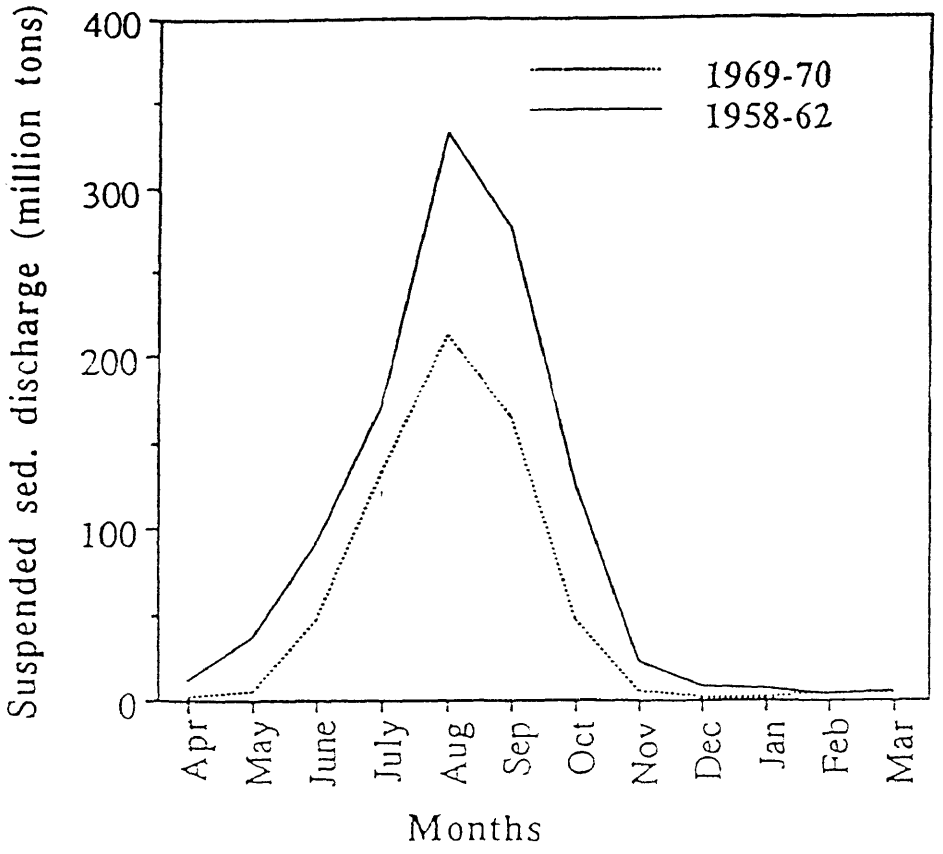

Figure 4 - Estimated monthly delivery of suspended sediment of the Ganges-Brahmaputra river system for a seasonal hydrologic cycle from April to March. The 1958-62 values are from Coleman (1969) and the 1969-70 values are from Bangladesh Water Development Board (1972) (from Barua et al., in press).

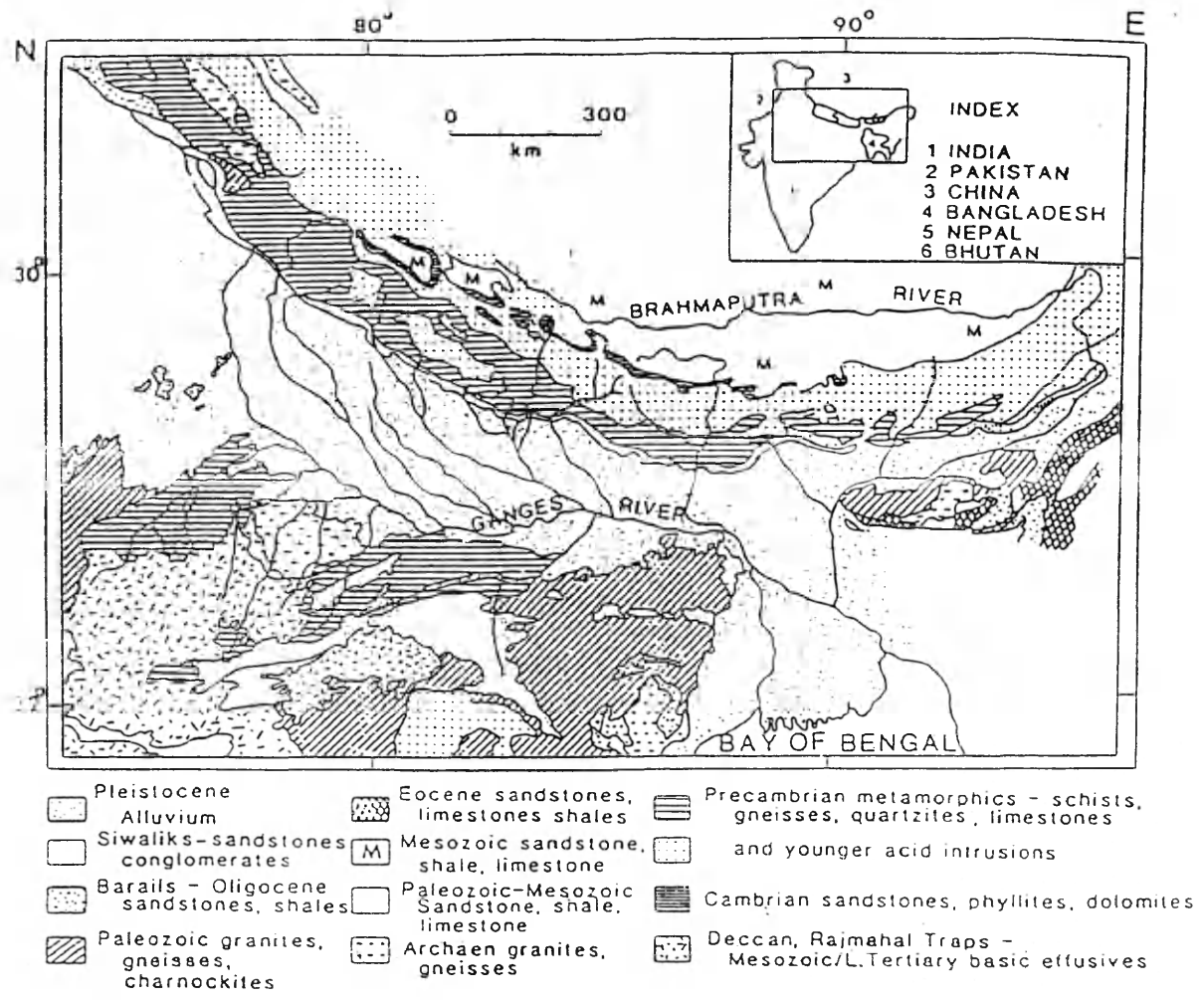

Figure 5 - Geologic map of the drainage basin for the Ganges and Brahmaputra rivers. The Ganges drains the Deccan and Rajmahal basaltic traps which is reflected in relatively high smectite concentrations for the clay-size sediment fraction (from Segall and Kuehl, 1992) .

Umitsu (1985, 1987, 1990) divided the landforms of the Bengal Basin into two geomorphological units: Pleistocene terrace uplands and recent alluvial lowlands (Fig. 6). The Pleistocene terraces are found in the marginal and interior portions of the Basin. In the north the uplands are known as the Barind Tract and as the Madhupur Jungle in the central region. Alluvial lowlands are distributed widely over the Bengal Basin. The alluvial lowlands are characterized by natural levees, point bars and channel bars as well as lower landform units such as swamps, marshes and former river channels. Sediments consist mainly of sand, silt, and clay layers with peat layers recognized in several places. The recent alluvial lowlands can be divided into the Ganges Delta, Brahmaputra-Jamna Flood Plain and Sylhet Basin. The elevation of the lowlands typically is less than 15 m above sea-level and most of the southern region is less than 3 m above sea-level.

Five stratigraphic units characterize the Holocene evolution of the Ganges subaerial delta since the last glacial maximum (Umitsu, 1990) (Fig. 7). The *lowest unit* dates from the last glacial maximum and consists of sandy gravels deposited by the rivers down cutting older surfaces. The upper contact of this unit is about 70 m below sea-level and Umitsu (1990) suggests that sea-level was probably at least 100 m below present during its formation. Radiocarbon dating

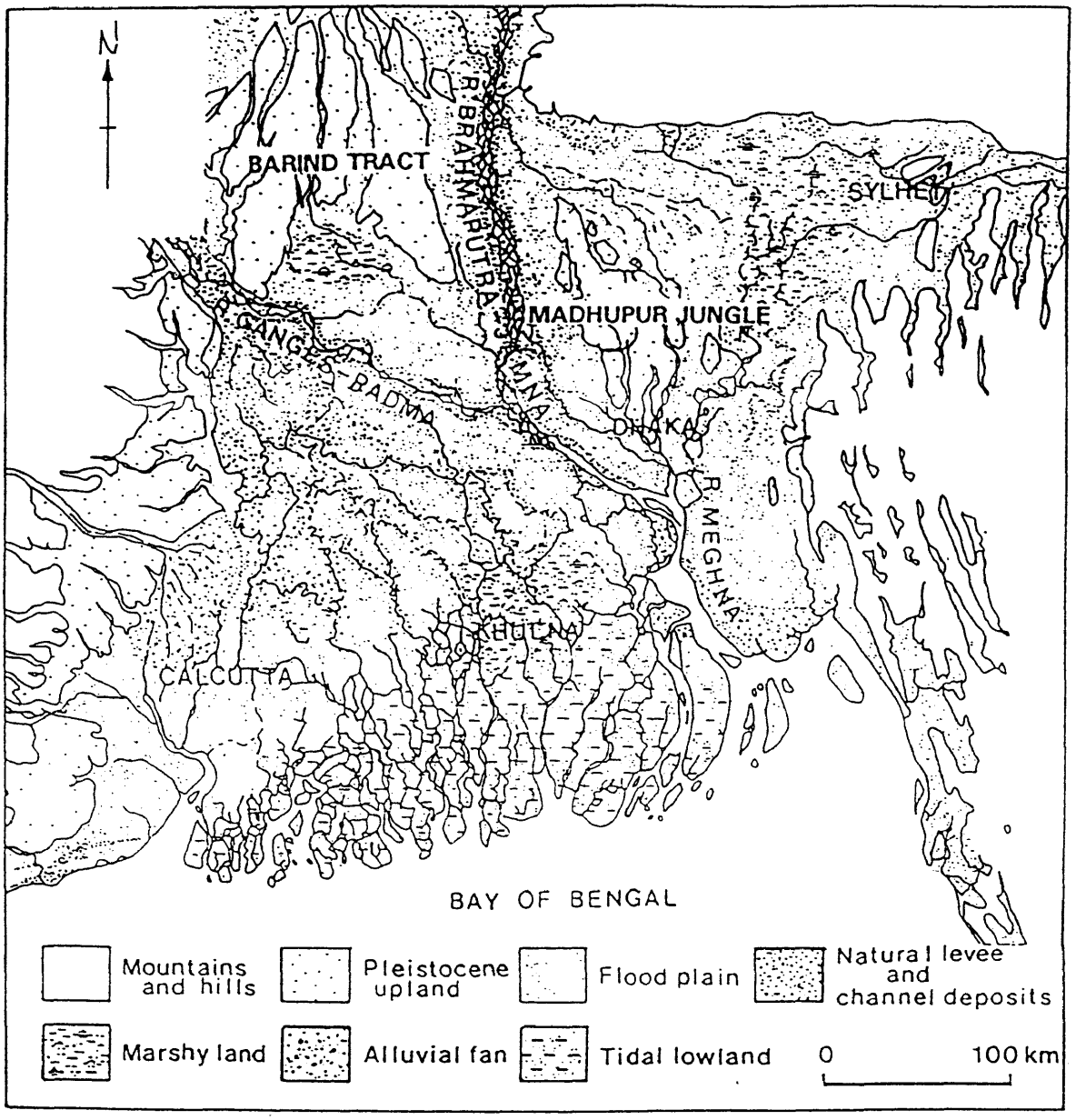

Figure 6 - Landforms of the Ganges-Brahmaputra subaerial delta plain/floor plain and surrounding regions (modified from Umitsu, 1990).

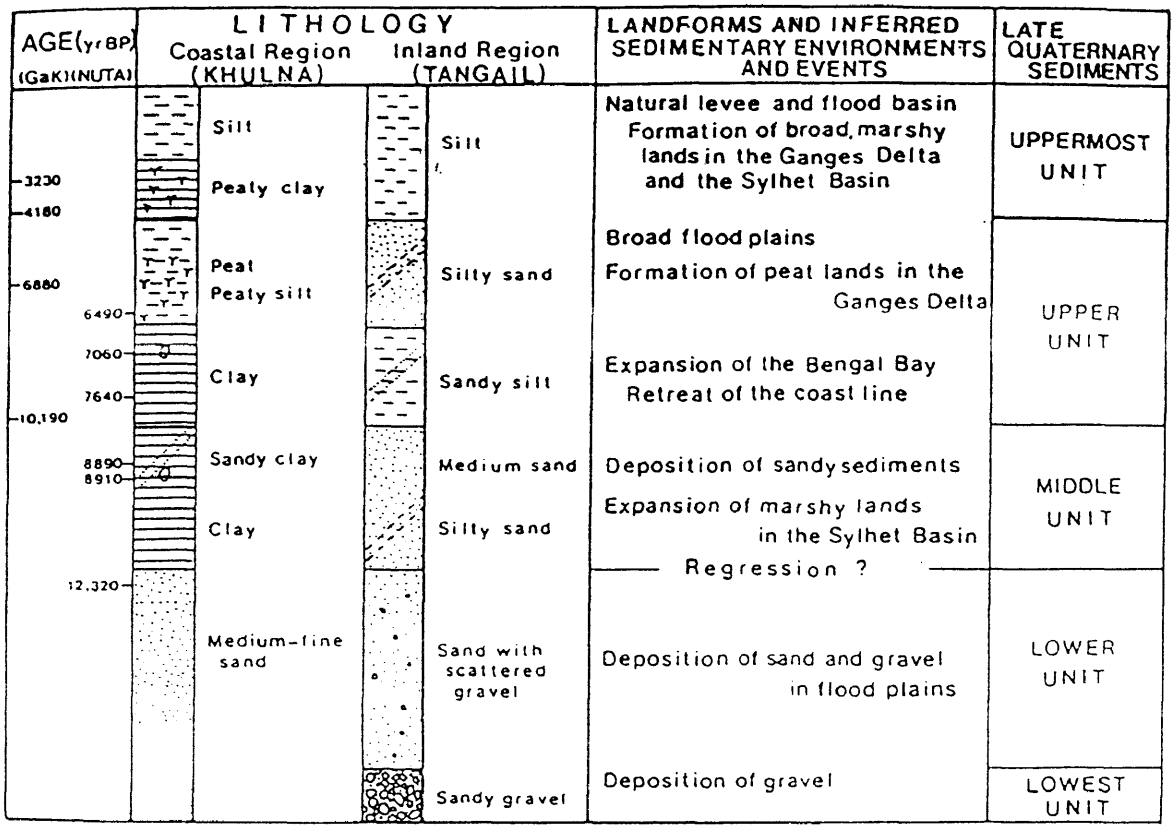

Figure 7 - Sedimentary environments and landforms in the Ganges delta, as interpreted from borings at Khulna and Tangail. Also shown are ^{14}C ages, lithologies, and inferred paleo-environments and events (from Umitsu 1990).

and similarities in sediment facies and grain size of the lower unit near Khulna City, with that of the present Brahmaputra River flood plain suggests that this unit was located in the flood plain about 12,000 years before present. The middle and upper parts of the unit are comprised of sandy sediments with scattered gravels. Between 12,000 and 10,000 years ago the surface of the delta became dissected with shallow valleys forming along the rivers. Umitsu (1990) theorizes that these valleys may be due to a temporary regression of sea-level. The *middle unit* is composed of fine deltaic sediments deposited during the transgression. Peat layers are found in the Sylhet Basin in the lower horizon of the unit showing the presence of marshes during this period. A fossil shell associated with areas of mangrove tree growth indicated this area was close to shoreline where mangrove trees once grew. During the middle Holocene the *upper unit* was deposited. The lower portion of the *upper unit* is comprised of silt and clay in the inland region of Tangail. Near the more coastal region of Khulna, the sediments exhibit a strong marine influence. Umitsu (1991) proposed that the coastline at that time retreated slightly north of the present Khulna City. The upper portions of the *upper unit* become coarser, with peat in places, suggesting that the coastline advanced toward the Bay of Bengal during this time as broad marshy peat lands covered the central Ganges Delta. During the late Holocene the

regression rate slowed allowing fine silts and clays with intermittent peat layers to be deposited, here called the *uppermost unit*.

Oceanography of the Indian Ocean and Bay of Bengal

The combined Ganges-Brahmaputra-Meghna river system discharges into an energetic marine environment characterized by strong tidal currents, moderate wave activity and seasonal monsoons. The impact of the mixing and subsequent spreading of the fresh water greatly affects the oceanography of the coastal ocean. In addition to the perennial discharges from the Ganges and Brahmaputra, seasonal discharges are introduced from India via the Godavari, Krishna and Cauvery Rivers (Suryanarayana, et al., 1992). The advection and mixing of these fresh waters (about 2300 km^3 per year) with the coastal ocean is controlled by internal and external forcing from wind and thermohaline conditions (Suryanarayana et al., 1992).

Seasonal low pressure areas over the Persian Gulf during the summer and high pressure during the winter over the Tibetan Plateau create monsoonal winds; from the southwest in summer and from the northeast in winter (Murty, et al., 1992). Changing monsoonal winds, affect surface water flow in the Bay of Bengal (Wyrtki, 1973). The spring is characterized by clockwise rotation, with

the fastest flow close to the central Indian continental shelf, where it can reach 3 to 5 knots. The autumn is characterized by counterclockwise movement with lower speeds in the eastern and central regions of the Bay as opposed to the western region. Spring winds, combined with the Coriolis effect, results in the movement of surface water away from the east Indian Coast in spring with deeper water upwelling, causing the isopycnals to tilt upward towards the Indian coast. In the autumn the reverse occurs as water is piled up in the western part of the Bay and the isopycnals tilt down toward the east Indian Coast. Resulting changes in sea level of 4 feet for the northeast coast at Chittagong and along southeast Pakistan are the largest on record (Murty, et al., 1992).

Tides in the coastal waters off Bangladesh primarily are semi-diurnal, with a range of up to 4 m (Barua et al., 1994) for a small area between Hatia and Sandwip channels near the river mouth and velocities exceeding 300 cm/s (Coleman, 1969). The combined effects of Coriolis acceleration and the funnel shape of the Bay is an area of increased tidal range along the eastern coast of Bangladesh, decreasing toward the west.

Sediment Dispersal to the Bengal Shelf

As a result of tidal asymmetry, net landward flow of sediment and water

during periods of low discharge occurs in the eastern-most channels of the delta system (Hatia, Sandwip and the eastern Meghna), whereas net seaward transport occurs in the more western channels (Tetulia, Shahbazpur and the western Meghna) (Fig. 8) (Barua, 1990). Some sediments entering flood channels may eventually be deposited in sheltered areas, stored in the migrating tidal flats, or ultimately escape to the open sea through ebb channels (Segall and Kuehl, 1992). Barua et al. (1994) show that the magnitude and distribution of suspended sediments during the low-discharge periods is primarily a function of tidal energy. Sediments which are 125 μm or less in size (fine sand-clay) are easily and continuously transported in suspension except for brief periods during slack water. Segall and Kuehl (1992) suggest that only during high-discharge periods (May-October) will significant amounts of sediment be transported to areas seaward of the 20 m isobath.

Based on examination of sedimentary structures and textures from cores and grab samples, Hariu (1988) identified three major sedimentary facies: 1.) inner shelf silts and sands extending from the coastline to the 25-m isobath; 2.) a thin (~0.5 m) veneer of inter-laminated silts and muds overlying the inner shelf silts and sands; and 3.) mid-shelf muds characterized by interbedded, faintly-laminated muds and slightly-mottled muds. Grain size analysis shows a fining to

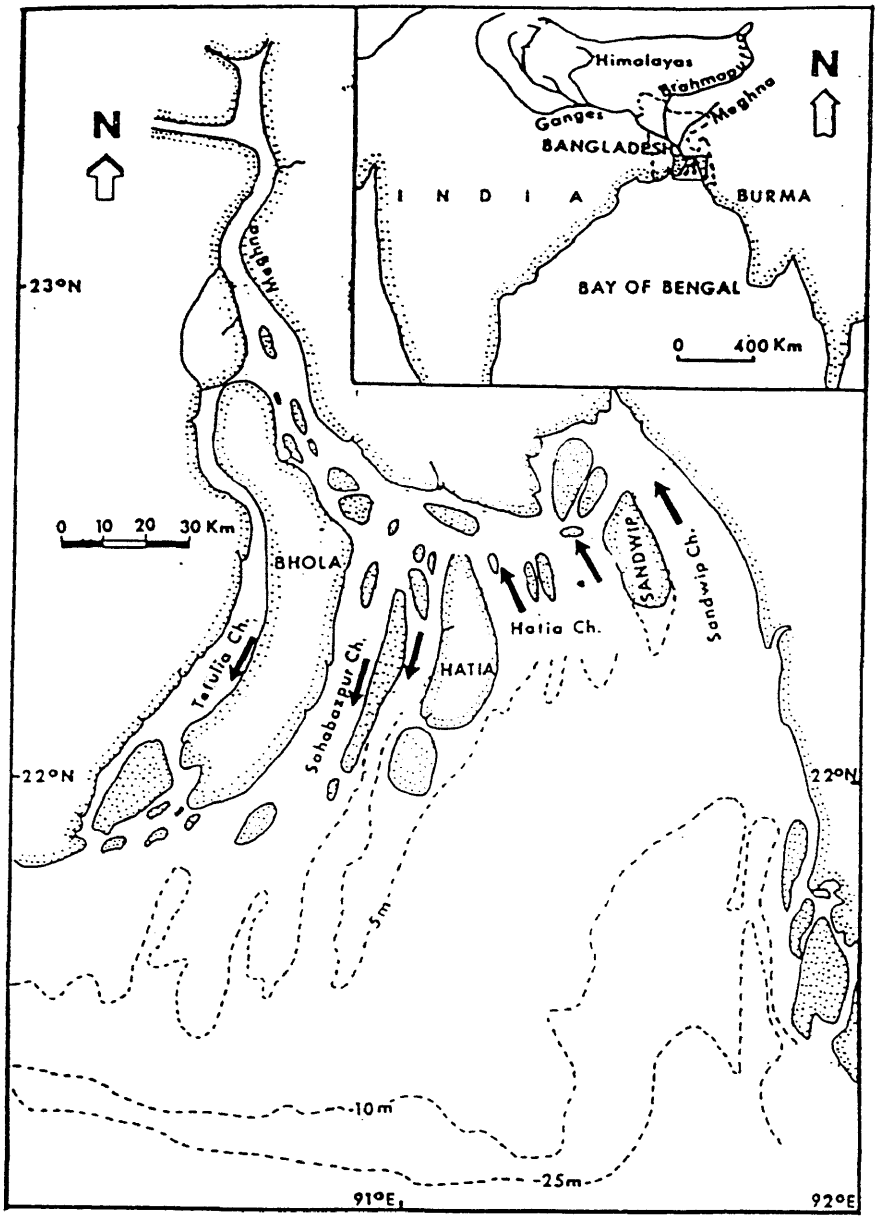

Figure 8 - The mouths of the Ganges-Brahmaputra-Meghna river system showing major flood and ebb channels (from Barua, 1990).

the west and increased sedimentation rates in the same direction, suggesting westward transport along the shelf toward the Swatch of No Ground (Kuehl et al., 1989). Flame structures and load structures, which represent penecontemporaneous deformation (indicating rapid deposition), are observed near the head of the canyon. Prior studies propose the canyon, which incises the area of highest sedimentation rates, may act as a conduit for off-shelf sediment transport (Kuehl, et. al., 1989).

Sediment Budget

A definitive sediment budget has not been determined for this river system, and several possible sinks for the sediment have been proposed. Umitsu (1993) presents evidence for sediment accretion on the flood plain and delta plain of about 50 m since the last glacial maximum. Based on more limited data, Coleman (1969) suggests that high tidal currents at the mouth prevent sediments from settling so that they are bypassed to the fan through the Swatch of No Ground. Kuehl et al. (1989) present textural, geochronological and clay-size mineralogical evidence which suggests that although a significant percentage of the sediment is trapped on the inner shelf, some bypassing through the canyon is occurring. However, investigations by Curray and Moore (1974), Curray et al.

(1982) and Emmel and Curray (1985) do not show evidence of recent sediment accumulation on the Bengal Fan.

Clearly, the fate of the sediments since the Holocene transgression is not conclusively known. Flood plain accretion (Umitsu, 1993), accumulation on the shelf and/or bypassing to the Bengal Fan via the Swatch of No Ground (Kuehl et al., 1989) have been suggested as sinks for the rivers' sediment; however, their relative importance has not been established. One of the goals of this thesis is to test the idea that subaqueous deltaic growth on the Bengal shelf accommodates much of the sediment load of the Ganges-Brahmaputra river system.

Methods

Field Methods

A total of 450 km of GeoPulse seismic reflection data was obtained from the Bengal Shelf during March 1991 along 8 transects (see Fig. 1) with maximum seabed penetration in excess of 100 m and vertical resolution of less than 0.5 m. Seabed sampling retrieved 9 kasten cores and 11 grab samples. In addition, cores and grab samples were collected on a previous cruise in 1987. Sediment cores were subsampled by taking centimeter-thick sections at various depths which were homogenized and bagged for sedimentological and geochemical analyses. A wood fragment was retrieved from the bottom of the kasten core from station 1 and was saved for radiocarbon dating.

Seismic Interpretation

Navigation data from the 1991 cruise was converted from Decca coordinates to latitude and longitude. Both horizontal and vertical scales were determined for the seismic profiles. Using a 3-point moving average in order to smooth variations, horizontal distances (in kilometers) for each transect were determined between each time mark, typically every 15 minutes. Vertical scales

were calculated based on the recorder setting, assuming a velocity of 1500 m/s.

The seismic profiles were analyzed both individually and collectively to identify and correlate distinctive features within the sediment wedge which provide insight to the nature of sediment accumulation on the Bengal Shelf. Areal extent of distinctive acoustic reflectors, erosional surfaces and overall geometry were determined. Spacing and thickness of reflectors was recorded along with the gradient of the beds. The overall slope of the sediment wedge was calculated between each time station and then averaged for inner-shelf, mid-shelf and outer-shelf breaks. Acoustic penetration was noted for possible correlations to grain size and natural gas deposits. Finally, key sections were digitally scanned to create figures. Scanned sections were cleaned, scaled, mosaicked and compressed as needed using **Intergraph Microstation™** and **IRASB™** vector/raster processing software.

Laboratory Methods

Radioisotope Analysis

Most of the radioisotope analyses were preformed using gamma spectroscopy. ^{210}Pb and ^{137}Cs activities were determined by the direct measurement of their characteristic gamma-ray emissions, whereas

measurements of ^{226}Ra/ ^{228}Ra were made indirectly through measurement of their daughter products. For cases where the parent is relatively long lived compared to the daughter, indirect measurement is possible utilizing the principle of secular equilibrium. Secular equilibrium is achieved when the rate of decay of the daughter is equal to that of its parent. Samples were packed in petri dishes (6.5 cm diameter by 2.25 cm), taped to prevent loss of ^{222}Rn (an intermediate daughter between ^{226}Ra and its measured daughters, ^{214}Pb and ^{214}Bi) and allow for ingrowth of the daughter isotopes, placed on the detector window and counted for 24 hours. Self absorption corrections for ^{210}Pb were made by placing a ^{210}Pb source atop the sample and counting for 200 seconds and then measuring the unattentuated beam intensity to correct for self attenuation (Cutshall et al., 1983).

Radiocarbon analysis was preformed on the wood sample using the benzene synthesis and liquid scintillation counting method described by Polach and Stipp (1967). The dried material was combusted in pure oxygen forming CO_2, which was passed over a chemical scrubber and two dry ice traps to remove impurities and water. A small aliquot of CO_2 was removed for $\delta^{13}C$ measurement using a ratio mass spectrometer to correct for isotopic fractionation. The remaining CO_2 gas was then reacted with molten Li metal to form LiC, which, through the addition of distilled water was converted to acetylene (C_2H_2). The

acetylene was then trimerized to benzene (C_6H_6) using an activated Cr catalyst. Scintillation cocktail was added and the sample was counted in a low-level scintillation analyzer for 1-2 days.

Grain-size Analyses

For textural studies the sample was wet sieved through a 63μ sieve to separate the sand and mud (clay and silt). Sand was sieved at 1/2 ϕ intervals and detailed analysis of the silt and clay fractions was preformed using a Sedigraph™ model 5100 ET x-ray digital settling analyzer. Analyses were combine to calculate mean grain size and sorting.

Results

Seismic Profiles

Subdivisions of the shelf were made based on significant breaks in slope or changes in acoustic charcteristic, for purposes of the following descriptions.

Near-Shore Region (5-15 m)

Seismic profiles from the near-shore region of the Bengal Shelf reveal a highly reflective sediment surface and few distinct subsurface reflectors (Fig. 9). In the northeastern section of the Bay, along the Chittagong coast, asymmetrical sand waves ranging in height from 3-5 m are seen. The sand waves appear to become more widely spaced toward the west in the direction of the lee face (Fig. 10).

Inner Shelf (15-30 m)

Seismic profiles reveal closely spaced acoustic reflectors (<2-3 m) located in the shallow seabed (upper 15 m). An irregular erosional surface below these reflectors in transects A and C can also be seen suggesting an areal extent of at least 720 km^2. This uneven erosional surface displays cut and fill features with

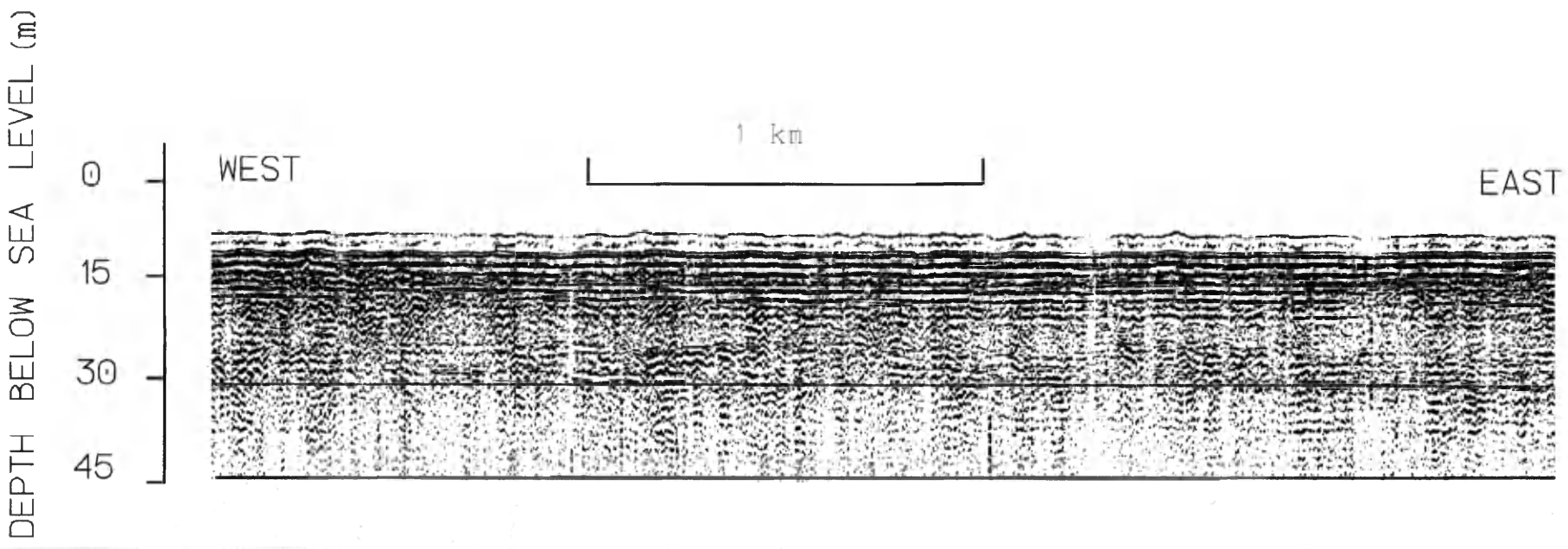

Figure 9 - Near shore seismic transect B, revealing poor penetration and loss of acoustic signal likely due to high sand content.

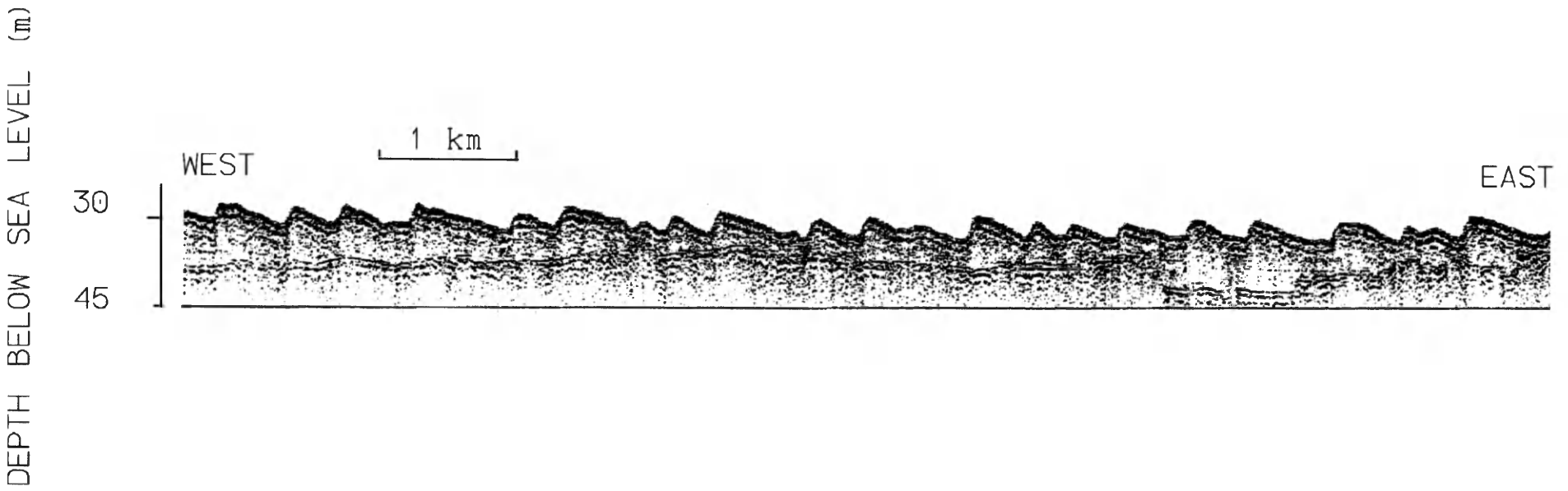

Figure 10 - Asymmetrical sand waves suggesting sediment transport to the west, from transect G near the eastern coast at Chittagong.

associated discontinuous and truncated bedding (Fig. 11).

The inner shelf dips gradually seaward in this region with an average gradient of 0.036°, with no significant change in gradient from east to west. Farther seaward, in water depths of approximately 30 m, greater than 30 m of sub-bottom penetration is achieved and previously-parallel reflectors begin to diverge. The spacing between reflectors increases with distance from shore, from <2-3 up to 5 m.

Middle Shelf (30-60 m)

Seismic profiles show densely spaced reflectors, typically 3-5 m apart. Thick sequences of these acoustic reflectors, between 30 and 45 m, are evident. The beds begin to converge seaward in water depths of about 60 m, where reflector spacing is reduced to <2-3 m. The gradient of the sediment wedge over the middle shelf is an average of 0.19°. This gradient appears to be uniform from the eastern transect to at least the Swatch of No Ground in the west.

Individual beds are difficult to discern in the seaward portion of the middle shelf and irregular, erosional surfaces can be seen below the stratified sediments. The erosional surface is uneven and displays varying relief, and underlying strata are mostly discontinuous with indistinct bedding.

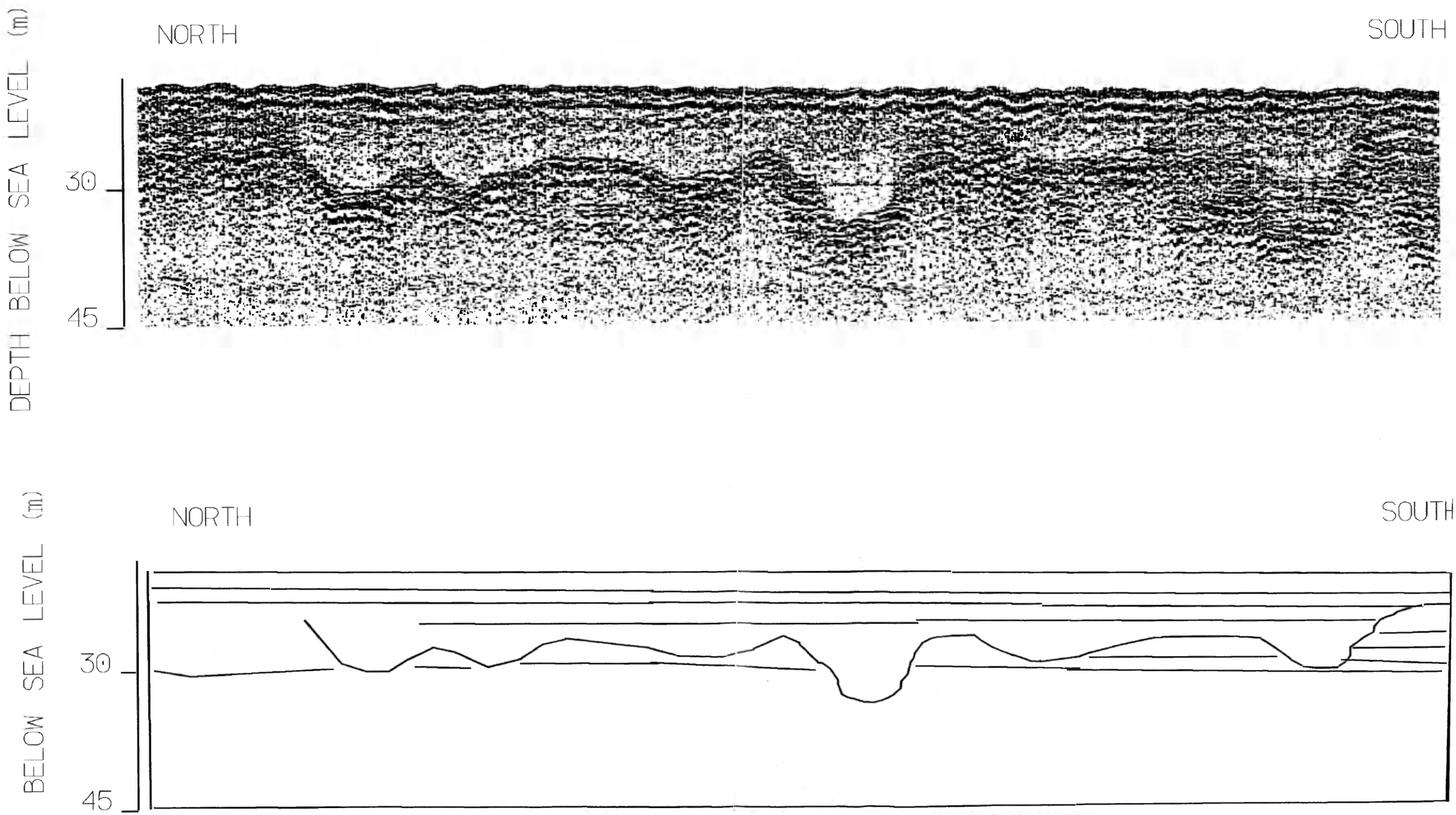

Figure 11 - Erosional surface from inner shelf (transect C) indicated by uneven surface and truncated bedding below near-surface stratified sediments.

Two distinct acoustically transparent layers parallel to the seabed are observed both from shore perpendicular and from shore parallel transects (Fig. 12). Located at depths of roughly 40 and 50 m below the sediment surface, the layers are roughly parallel to one another, are spaced about 10 m apart and range from 3-5 m in thickness. As the mid shelf region dips seaward the transparent layers follow the same gradient within the sediment wedge until they pinch out toward the outer shelf at depths of about 80 m. Based on the seismic data, the layers appear to have an areal extent of at least 1500 km^2, extending at least 12 km north-south and 127 km east-west.

Outer Shelf (60-80 m)

Profiles in the outer shelf region show closely spaced (<2-3 m), parallel acoustic reflectors extending to water depths of at least 80 m, the seaward extent of the seismic lines. Slope in this area is very gentle, 0.022°. An erosional surface is seen below the shallow strata relatively close to the surface (within ~10 m). Distinct cut and fill structures are revealed in the uneven erosional surface (Fig. 13).

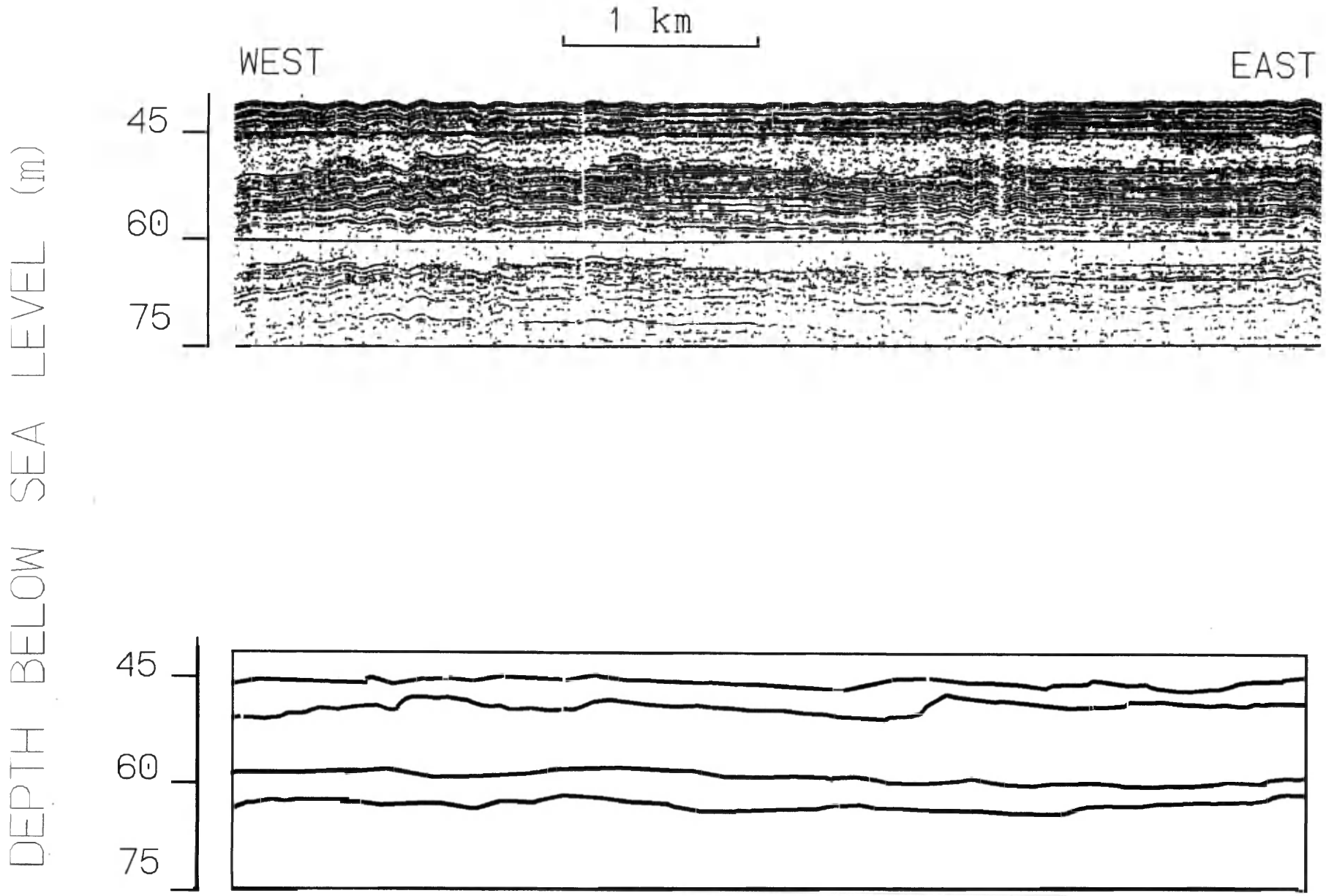

Figure 12 - Acoustically transparent beds from transect E, possibly the result of storm events in the Bay of Bengal.

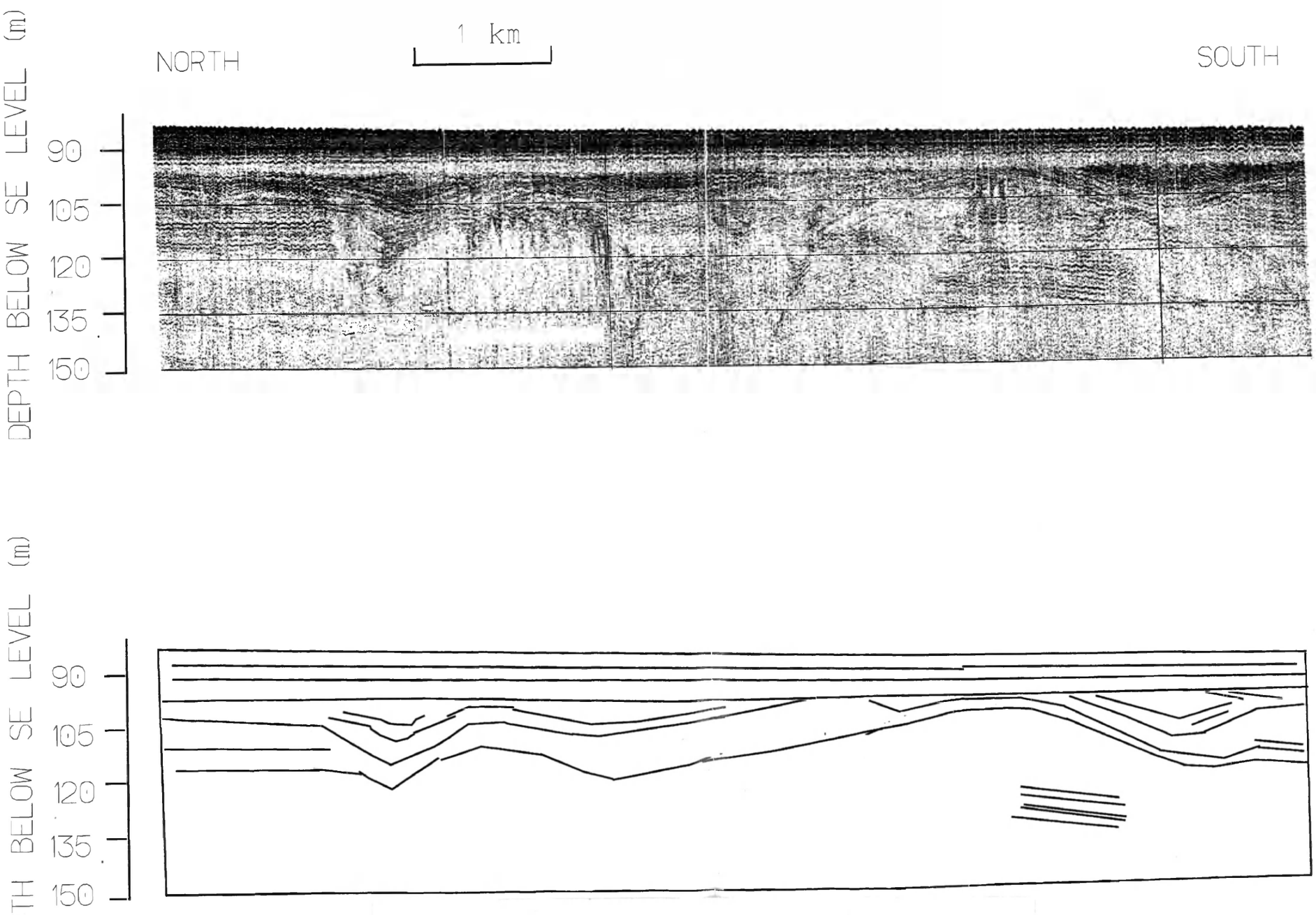

Figure 13 - Erosional surface below nearly horizontal near-surface reflectors, note cut and fill structures suggesting relic gullies and channels. From transect C.

Swatch of No Ground

Seismic profiles near the Swatch of No Ground reveal increased acoustic penetration in contrast to the far eastern and near-shore regions (Fig. 14 and 15a & 15b). On the western side the seabed is well stratified and reveals the most distinct, parallel, and continuous acoustic reflectors found in the sediment wedge, with typical spacing of 3-5 m between beds. For this side of the canyon, 60 m of acoustic penetration was achieved, with reflectors apparent throughout. On the eastern side of the canyon, beds are also densely spaced and but are more irregular in nature than their western counterparts. Below the thick sequences of stratified sediment lies an irregular erosional surface characterized by discontinuous and uneven beds of varying relief.

Growth faults and slumps are found on the flanks of the canyon. On the eastern side, slumps with rotational movement (Fig. 14) are noted that are slumping to the west, into the canyon. Also on the eastern side of the canyon, an east-west trending gully feeding the canyon is seen with growth faults along the south side dipping steeply into the canyon (Fig. 15). Near the head of the canyon, strata become more irregular but remain very thick. Strata are uneven and often chaotic, with discontinuous and truncated beds. Profiles of the canyon floor near its head show thick, irregular strata and an uneven sediment surface

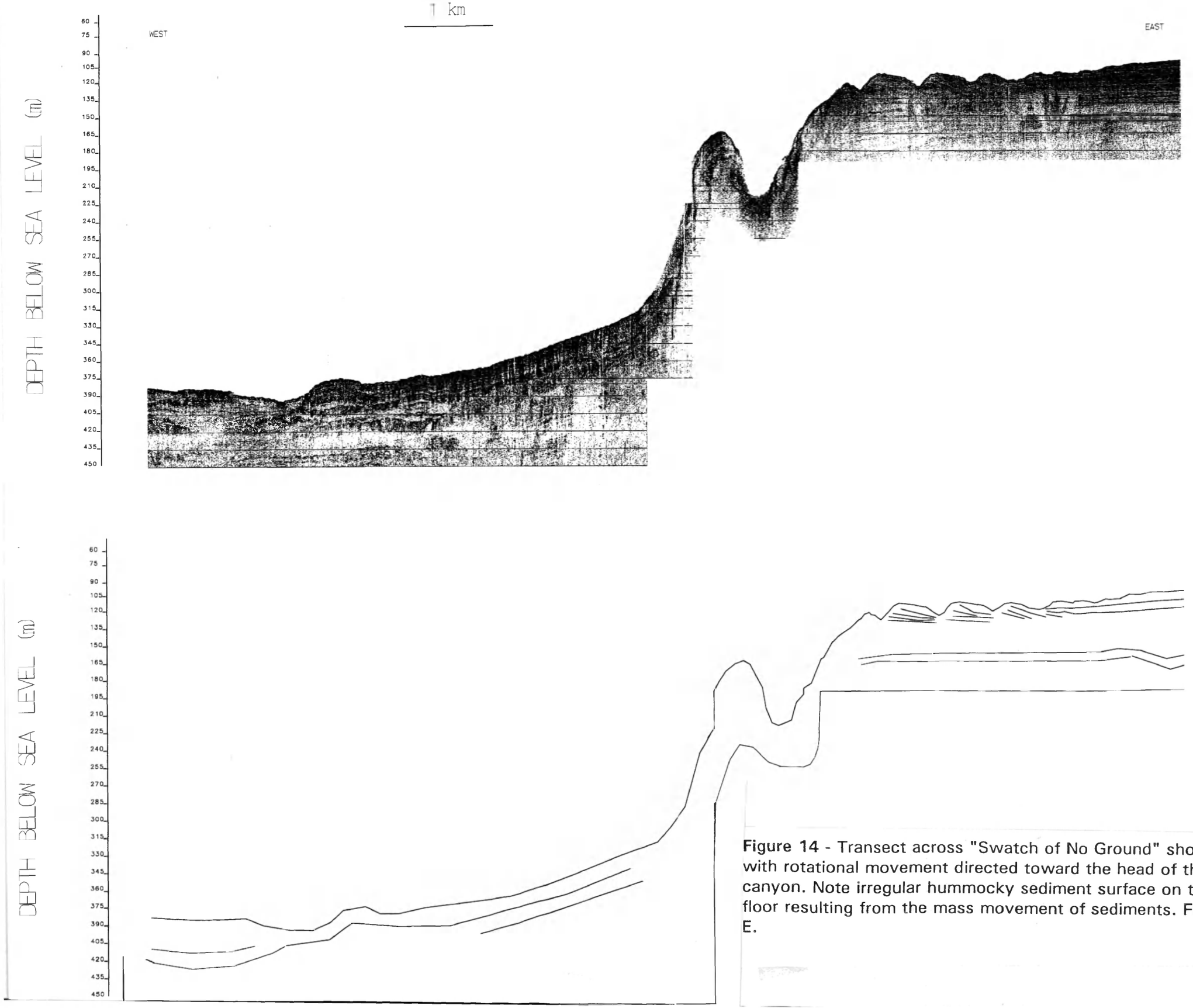

Figure 14 - Transect across "Swatch of No Ground" showing slumps with rotational movement directed toward the head of the submarine canyon. Note irregular hummocky sediment surface on the canyon floor resulting from the mass movement of sediments. From transect E.

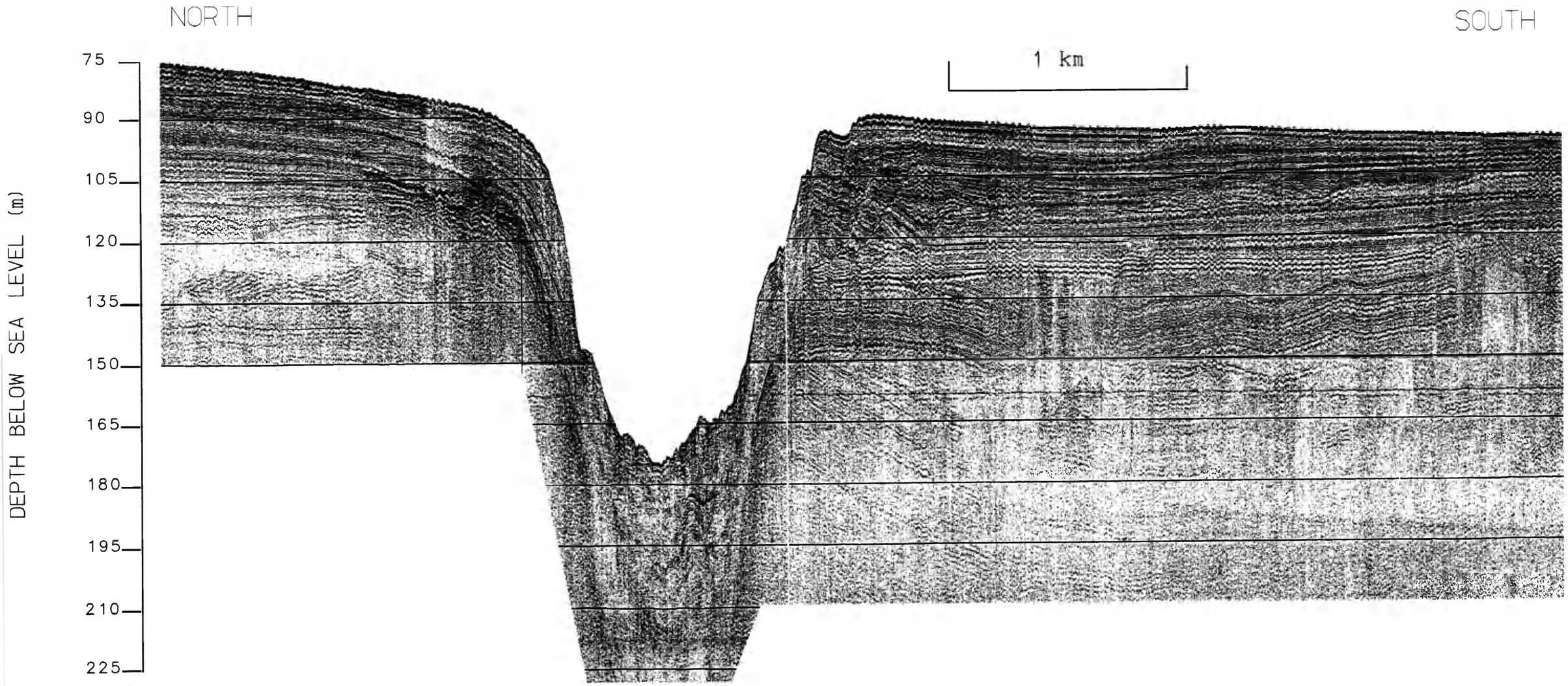

Figure 15 - Growth faults near a gully feeding the Swatch of No Ground, note irregular hummocky sediment surface at bottom of gully, suggesting mass movement and subsequent channeling through the Swatch of No Ground. From Transect D.

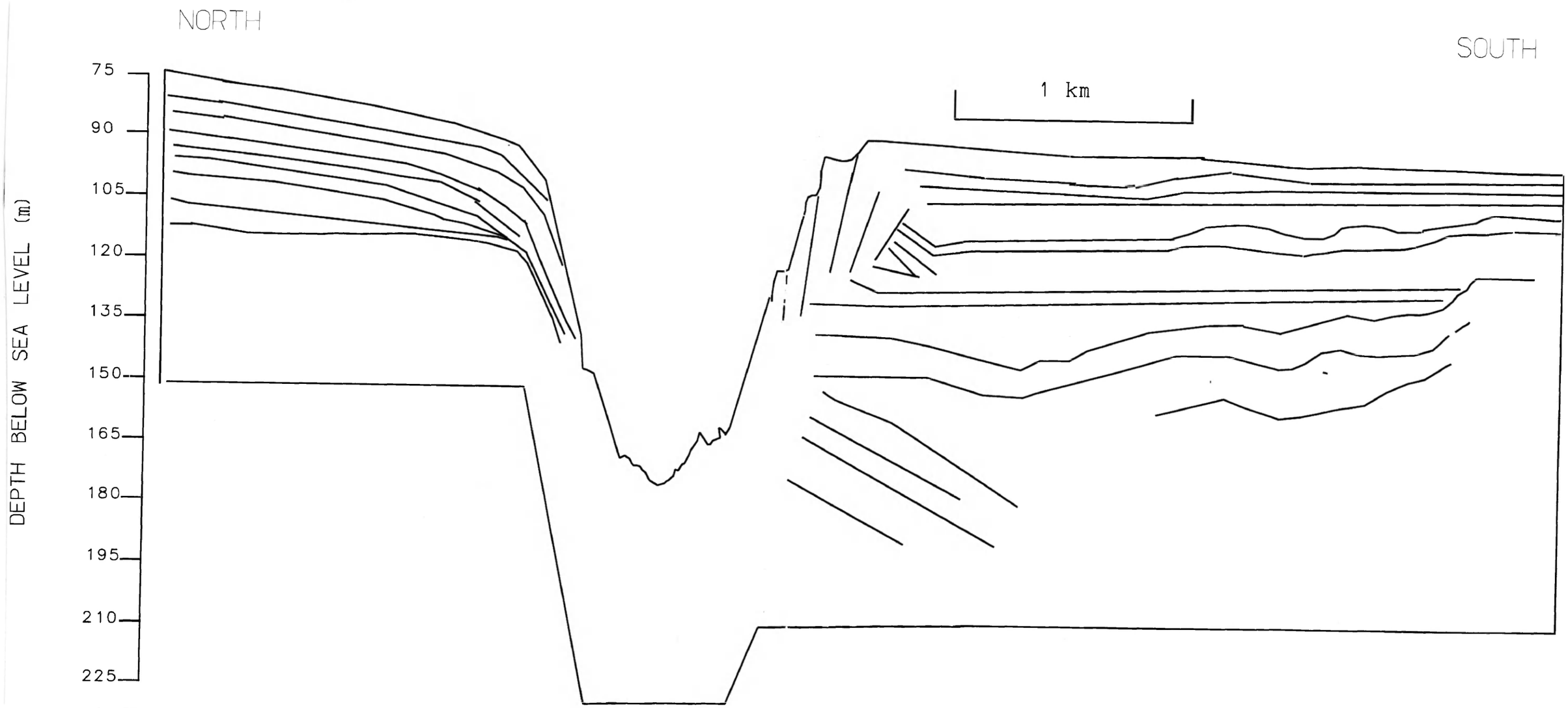
NORTH
SOUTH
1 km
DEPTH BELOW SEA LEVEL (m)
75
90
105
120
135
150
165
180
195
210
225

with few discernible beds.

Sediment Accumulation

All cores analyzed in the present study for short-lived radioisotopes revealed recent accumulation. Utilizing ^{137}Cs, a sediment accumulation rate of 1.9 cm/yr is derived for the near shore area (core 9). This rate could be a minimum because the ^{137}Cs levels are present throughout the core, thus the actual first appearance of ^{137}Cs in the seabed could be deeper. Alternatively, if deep physical mixing (>60 cm) affects the seabed in this area, the penetration depth could reflect this mixing and long-term accumulation rates could actually be lower.

On the mid shelf, a sediment accumulation rates of 1.2 cm/yr (core 6) and 0.9 cm/y (core 4) were derived using ^{137}Cs. These rates, also, likely are maximum, because the depth of first appearance is recorded, but may be artificially deepened due to mixing.

The highest sedimentation rates are found in areas surrounding the Swatch of No Ground. From core 5 a minimum rate of 5.5 cm/yr derived from ^{137}Cs, and a rate of 12.1 cm/y is derived using $^{228}Ra/^{226}Ra$. In order to apply $^{228}Ra/^{226}Ra$ in this area (core 5) (Fig. 16), two basic assumptions were made:

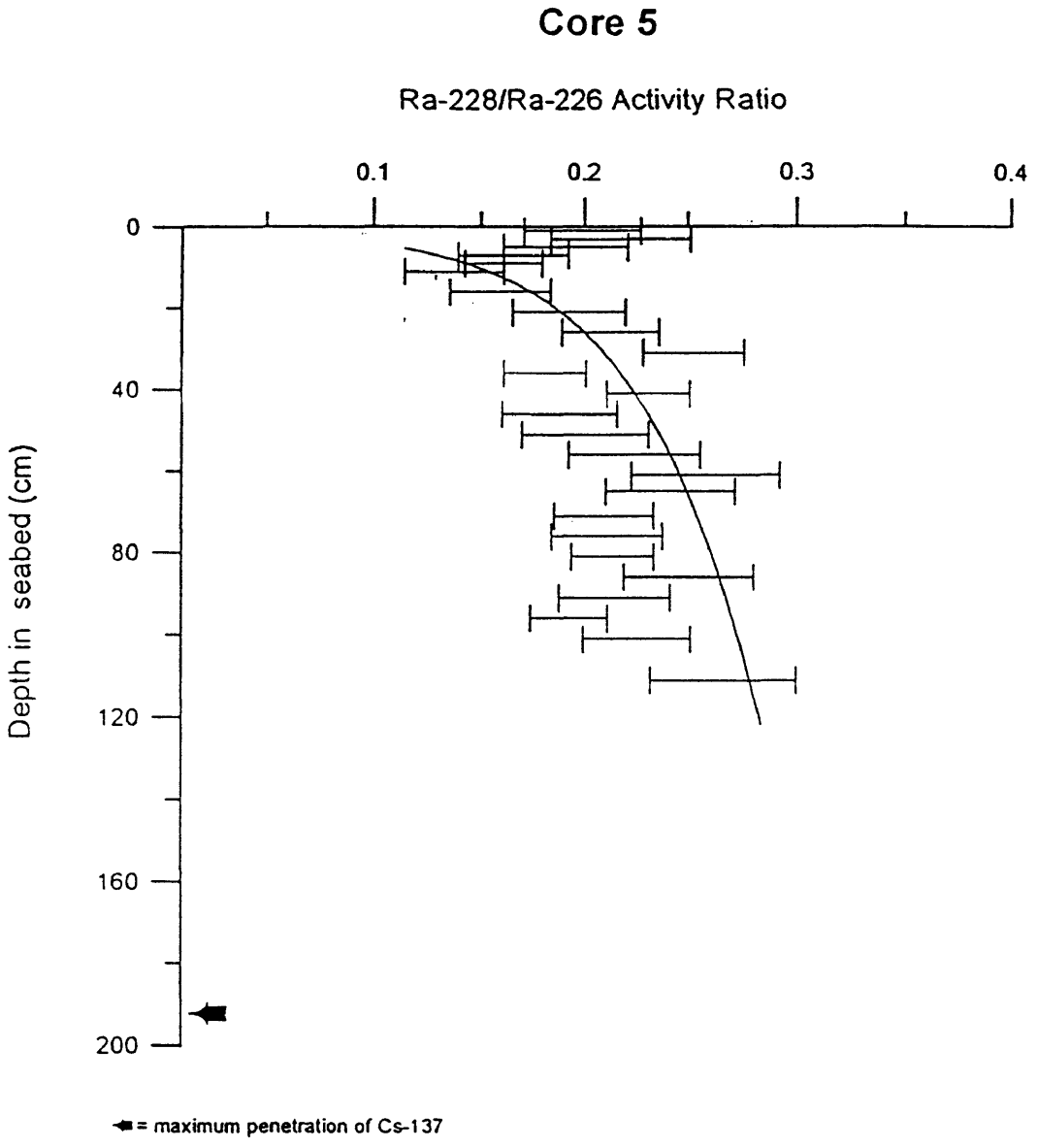

Figure 16 - $^{228}Ra/^{226}Ra$ activity ratio profile for core 5

secular equilibrium between ^{228}Ra and it's parent ^{232}Th is achieved at some depth and negligible ^{228}Ra diffusion occurs. ^{137}Cs supplies a convenient time marker to determine the depth where ^{228}Ra has reached equilibrium because its relatively recent introduction to the atmosphere (~ 35 years) closely matches five half-lives of ^{228}Ra (~30 years) needed to achieve secular equilibrium . This amount of time is not enough for the relatively longer-lived ^{226}Ra to ingrow appreciably. Unfortunately, core 5 is too short to record the first appearance of ^{137}Cs, and thus the maximum penetration. Another nearby core (core 4) with a complete ^{137}Cs profile is assumed to be a good representation of core 5. Therefore, core 4 was used to supply the ^{232}Th activity level necessary for the calculation of accumulation rates (see equation in appendix B) . A large error is inherent in this calculated rate, because the core used for ^{232}Th activity levels is a proxy for core 5, from which the actual $^{228}Ra/^{226}Ra$ activity ratios are obtained. In addition the ^{232}Th levels are an average from below the depth of maximum Ra diffusion.

For the outer shelf, sediment accumulation rates were derived using both ^{137}Cs and ^{210}Pb profiles from core 1. Large fluctuations in excess ^{210}Pb activity levels in the inner- and mid-shelf areas and the Swatch of No Ground preclude the use of ^{210}Pb as a geochronometer, but it may be applied here (Fig. 17). A

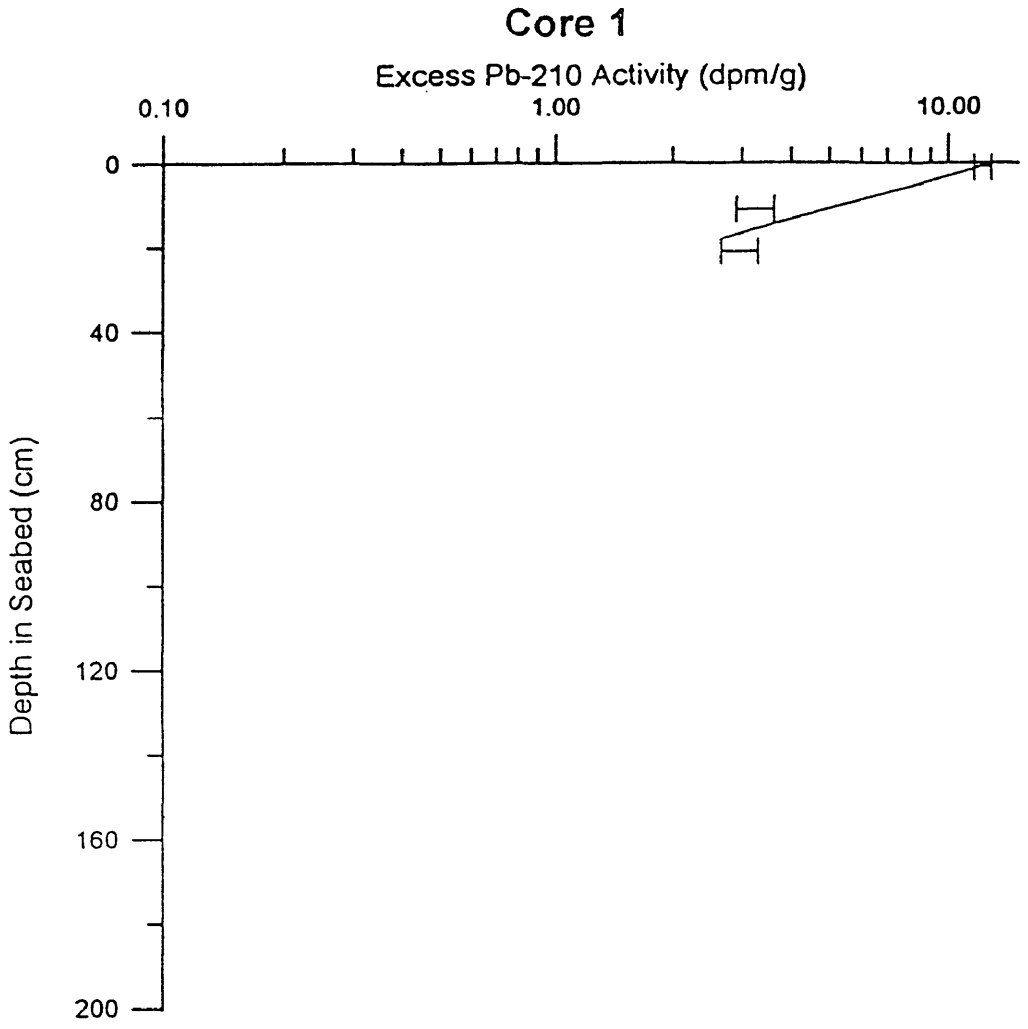

Figure 17 - ^{210}Pb excess activity profile for core 1. sedimentation rate of .

maximum sediment accumulation rate of 0.3 cm/yr was derived from both ^{137}Cs and ^{210}Pb activities.

Grain-size Analysis

Down-core analysis of grain size (see Appendix E) reveals the mean grain size for each sampling interval as well as a whole-core average. Mean grain size for the near shore area (station 9) is 7.6ϕ. Averages for the mid-shelf range from 7.0ϕ(station 8) and 7.9ϕ (station 6) to 8.5ϕ (stations 4 and 5) farther west near the Swatch of No Ground. Station 1 in the outer region has an average mean of 7.9ϕ (see Fig. 1 for station locations).

Discussion

Subaqueous Delta

A distinctive morphology can be seen in the sediment wedge prograding southward and westward from the rivers mouths on the inner Bengal Shelf (Figs. 18 and 19). The seismic profiles reveal the gently sloping topset, more steeply dipping foreset, and gently sloping bottomset stratigraphy characteristic of subaqueous deltas prograding off the Amazon and Huanghe rivers (Nittrouer et al., 1986; Prior et al., 1986). On the inner shelf, in water depths of about 15-25 m, reflectors are nearly parallel and slope gently seaward. This trend gives way to divergent beds at the seaward edge of the topset region, evidenced by increased spacing between reflectors and increased sedimentation rates (from 2 to about 12 cm/y). At depths of roughly 30 m the seafloor gradient increases abruptly (from 0.036° to 0.19°) and reflectors converge seaward across the foreset region. Toward the seaward edge of the foreset beds, sedimentation rates decrease to between 1.2 and 0.9 cm/y. In the bottomset region (>60 m water depth) near-surface reflectors once again take on a semi-parallel appearance with strata that are closely spaced and thin. The bottomset region has the lowest sedimentation rates (<0.3 cm/yr) found on the subaqueous delta.

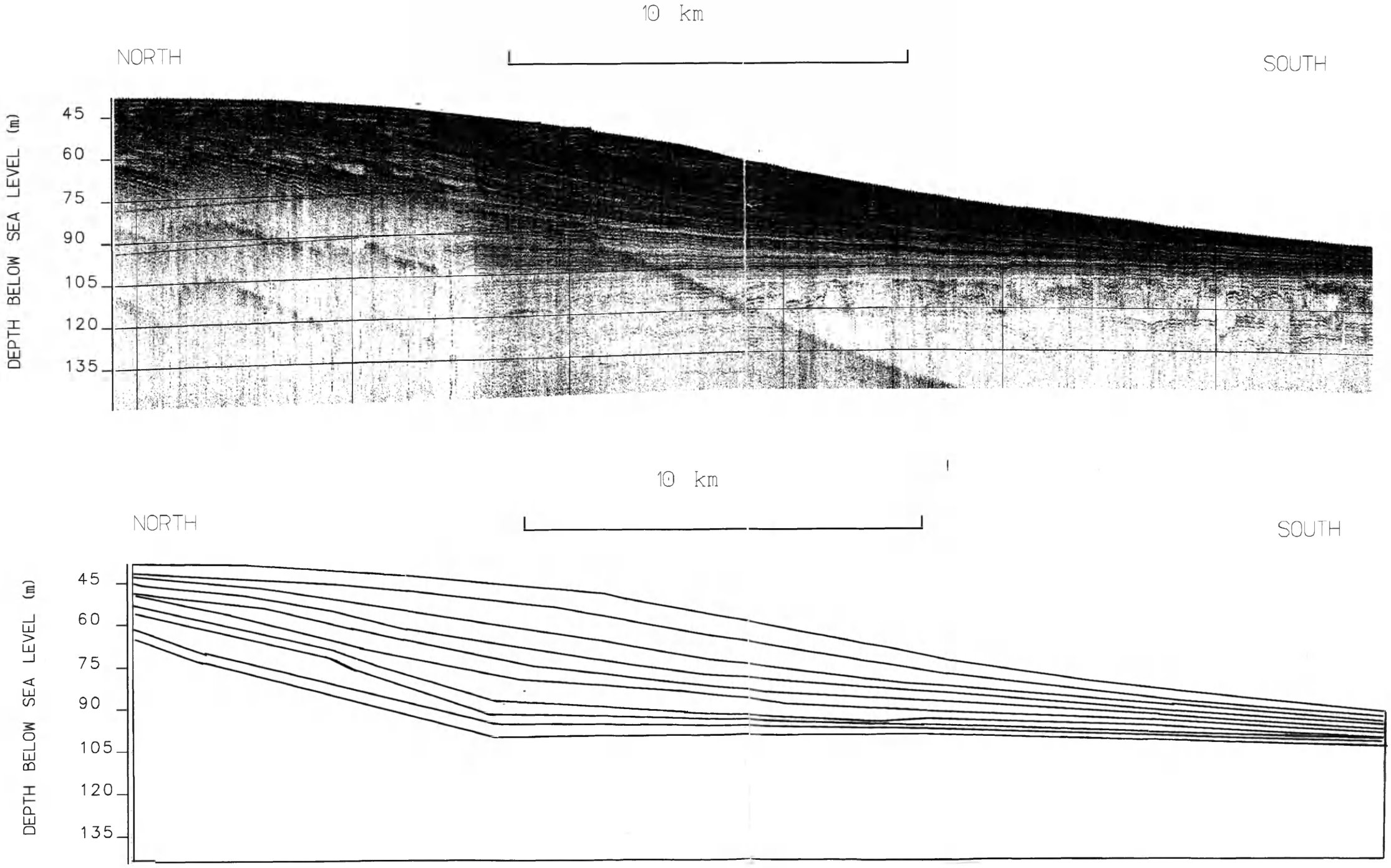

Figure 18 - Profile of sediment wedge seaward of the rivers mouths revealing clinoform structure with characteristic diverging topset, converging foreset, and parallel bottomset stratigraphy. From transect A.

VITA

Beth Michele Levy

Born in Brooklyn, New York August 1, 1971. Graduated from Tottenville High School in 1989. Earned B.A. in Geology from the University of Colorado at Boulder in 1993. Entered Master of Arts program in the College of William and Mary, School of Marine Science in 1993.

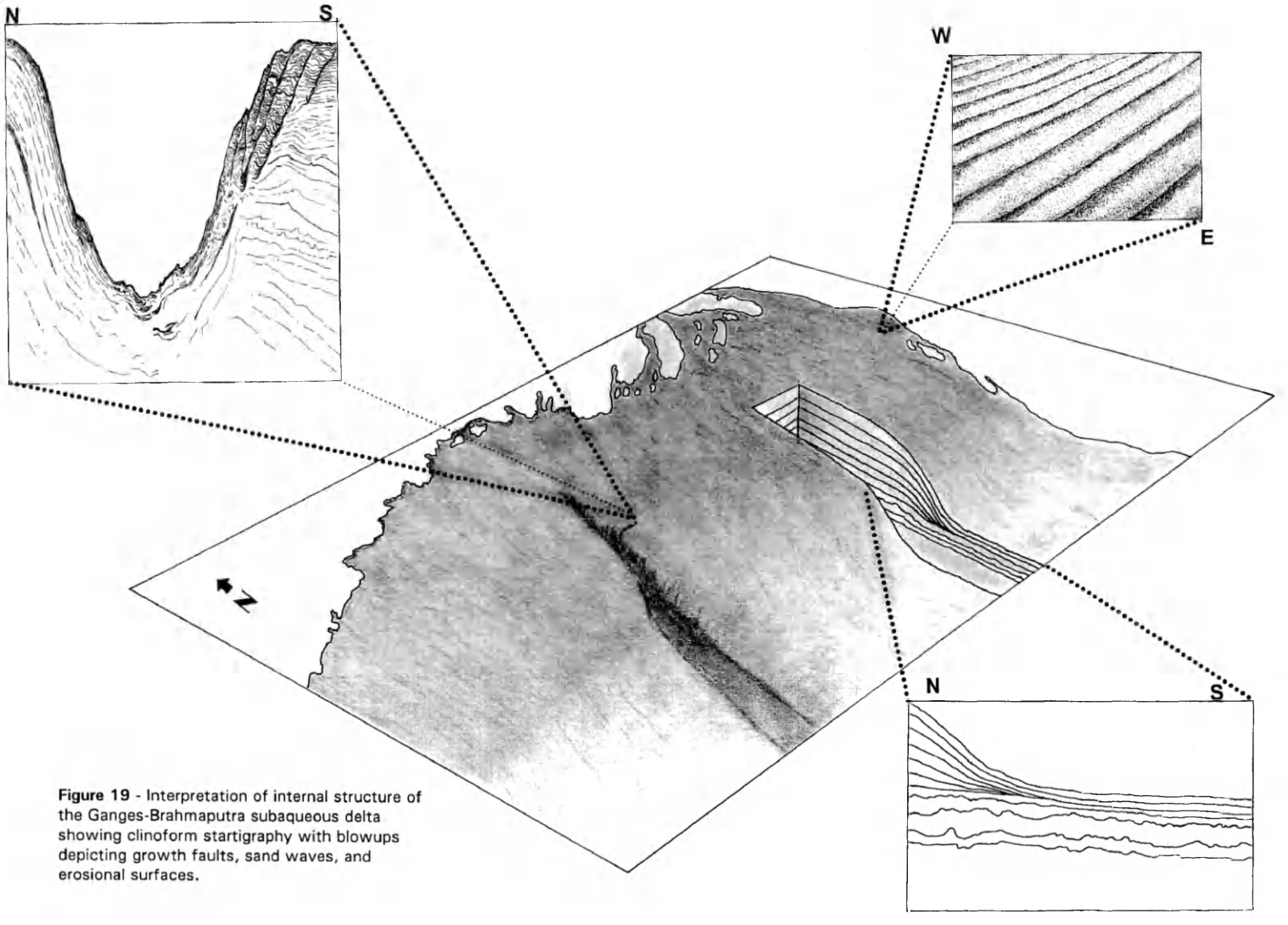

Figure 19 - Interpretation of internal structure of the Ganges-Brahmaputra subaqueous delta showing clinoform startigraphy with blowups depicting growth faults, sand waves, and erosional surfaces.

An erosional surface is also seen below the bottomset beds with evidence of uneven truncated bed and relict channels. Here the erosional surface is visible close to the surface. A wood fragment dated at ~12,000 years is found at the base of core 1 from this region suggesting this surface is most likely Pleistocene in age.

The Swatch of No Ground incises the mid shelf in the western foreset region, the area of highest sedimentation rates (up to 12 cm/yr). Evidence of penecontemporaneous deformation of strata is common in areas surrounding the canyon. High rates of sediment deposition are one cause of sediment failures such as growth faulting, slumping, and mud flowage (Fig. 14 and 15). Slumps and growth faults near the margins of the canyon and uneven, hummocky strata at the base of a gully feeding the Canyon and on the main canyon floor suggests sediment is being channeled off-shelf through the canyon. X-radiographs from cores taken during the 1987 cruise show flame structures and load structures near the head of the canyon (Hariu, 1988). Thus, both large and small-scale structures suggest sediment being deposited with penecontemporaneous deformation, indicative of rapid sedimentation.

Within the subaqueous delta two distinct, acoustically-transparent layers are seen in the mid-shelf area, in sharp contrast to the surrounding well-stratified

sediments (Fig. 12). These transparent layers extend at least throughout the central portion of the clinoform and follow the slope of the subaqueous delta. They have an areal extent of ~1500 km^2 and appear to be confined to the eastern side of the Swatch of No Ground. A possible explanation for these transparent layers is that they represent large-scale mud flows similar to those observed off the Mississippi River (Wright and Coleman, 1974). The widespread nature of these features suggest large-magnitude external forcing for failure. Such forcing could be accomplished by cyclones common to the study area.

Shelf Sediment Dispersal

Sediments appear to be transported southward and westward toward the Swatch of No Ground reinforcing previous studies by Rao (1964), Hariu (1988), Rao et al. (1988), and Kuehl et al. (1989). Energetic waves and tidal currents at times of maximum sediment discharge likely prevent rapid accumulation of sediments near shore. Westward transport is evidenced by a fining trend of sediment toward the west, directional evidence from sand waves and increased sedimentation rates near the Swatch of No Ground.

Textural characteristics of the seabed provide insight into the flow direction of sediments discharged to the shelf. Sediments display a fining trend

southward and westward toward the Swatch of No Ground. For example, foreset beds in the east have whole-core average grain size of 6.9ϕ (station 8), whereas station 6, (farther west) on the outer foresets is finer at 7.9ϕ. The most western stations (4 and 5) near the Swatch of No Ground, have average grain sizes of 8.5ϕ.

In the near-shore region, sand waves are found along the eastern margin, near the coast of Chittagong. Field descriptions of grab samples from this area reveal a clean medium sand. The sand waves have considerable relief (3-5 m), implying a high energy environment. Toward the west, these features disappear, but the poor acoustic penetration achieved in the profiles suggest relatively coarse grain size. The orientation of lee and stoss sides of sand waves indicates east to west flow direction (see Fig. 10).

Poor acoustic penetration (<25 m) on the inner shelf hinders detailed stratigraphic analysis. Possible reasons for this are coarser grain size and spatially restricted areas of gas deposits which interfere with penetration of the acoustic signal. In the area where sand waves are found, almost no acoustic penetration is achieved and individual beds cannot be discerned. In profiles from the Swatch of No Ground, thick sediment sequences are visible, beds are distinct and acoustic penetration approaches 100 m. The increased penetration likely

results from a fining in grain size, and increased water content. The Swatch of No Ground appears to divert the flow of sediments into the Canyon. The existence of growth faults and slumps directed into the canyon, coupled with the irregular, thick sequences of sediment found at the bottom of the canyon, suggests that sediment is bypassing the shelf via the Swatch of No Ground, presumably to the Bengal fan.

Volume of Holocene Sediment Wedge

The volume of the sediment wedge forming on the inner shelf was calculated using **SURFER**™ (Table 1; Appendix G). Volume determinations for sedimentation since the Holocene transgression were made using two different scenarios, dividing

AREA	VOLUME (m^3)
Marine to Swatch of No Ground	1.68×10^{12} +/- 0.8%
Marine to Hugli River	1.97×10^{12} +/- 0.8%
Terrestrial to Swatch of No Ground	0.22×10^{12} +/- 1.1%
Terrestrial to Hugli River	0.26×10^{12} +/- 1.1%

Table 1. Volumes from surfer calculation separated using two different western boundaries, the Hugli river and the Submarine Canyon, the Swatch of No Ground. Errors represent deviations from three methods used to calculate volume (see Appendix).

marine and terrestrial material. This is done to distinguish between the component of marine sedimentation since the Holocene transgression (the subaqueous delta) and the component accommodated in the flood plain (terrestrial). In addition to using surficial geologic maps to determine the areal boundaries for these estimates, cores described by Umitsu (1990) and his interpretations regarding Quaternary environments and landforms of the Ganges-Brahmaputra delta were used. Extrapolation of Umitsu's cores to the off-shore seismic data in this study enabled estimates of the thickness of the subaerial and subaqueous components of Holocene sediments comprising the Ganges-Brahmaputra delta to be made.

The Khulna region is considered the inland extent of the Ganges-Brahmaputra delta shoreline during the Holocene (Umitsu, 1990). The stratigraphy is characterized by a surficial clay layer approximately 10 m thick, topping a 10-15 m silt layer which in turn overlies 15-20 m thick sand layer. This presence of clays and silt over an underlying sand layer suggests a transgression. Two fossil molluscs, *Corbiculidae geloina* and *Neritiolae neritina,* found at a depth of 16 m suggest this area was once a tidal environment. Radiocarbon dating of wood fragments found in the core at a depth of 16 m

below sea level reveal an approximate age of 7,000 years before present (Umitsu, 1990).

The landward boundary for the combined terrestrial and marine portions of the delta is extrapolated laterally from Khulna for the volume estimates (Fig. 20). In the east, the coast along Burma provides a natural boundary. A southern boundary is provided by the 80 m isobath; bottomset beds are thin at this water depth, and immediately overly the Pleistocene surface. ^{14}C dating of a wood fragment from the base of core 1 (140 cm), from 80 m water depth provide an age of approximately 10,000 BP. Thus the seabed surface at 80 m water depth is a close approximation of the seaward boundary. Two different situations are considered regarding the western boundary (Fig. 21). The first assumes that the Swatch of No Ground interrupts sediment flow from the combined Ganges-Brahmaputra river system and acts as a western limit for the subaqueous delta. The second assumption takes into account the possibility that sediment is being deposited on the western side of the canyon, presumably from the Hugli river, just to the west of the Swatch of No Ground, which was a major outlet for the Ganges River in recorded history. Volumes of terrestrial and marine areas of the delta were determined separately. The area north of the modern coastline to the inferred 7,000 BP coastline at Khulna is defined as

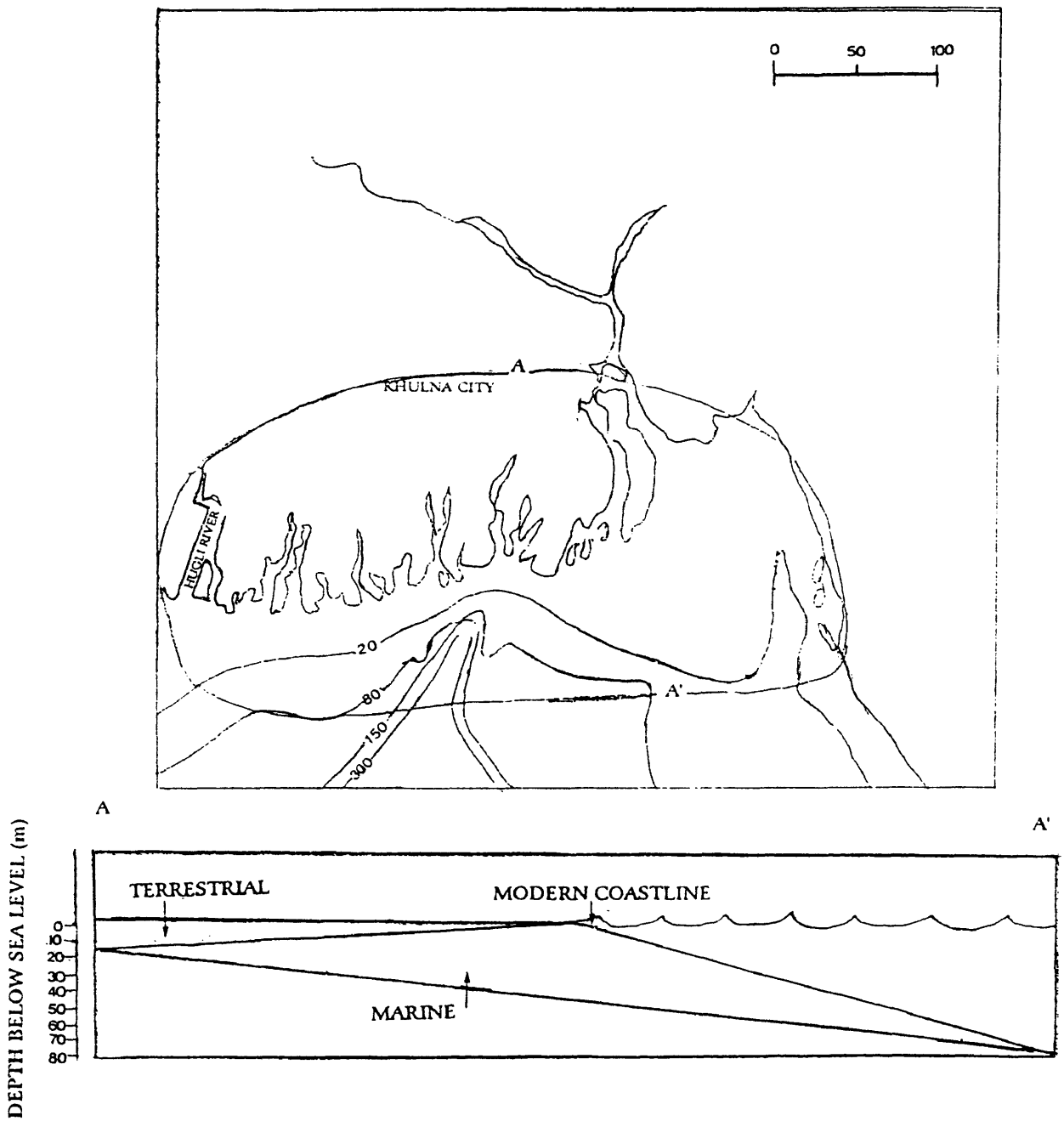

Figure 20 - Map showing the areas used for determination of the volume of Holocene sediment divided into marine and terrestrial components.

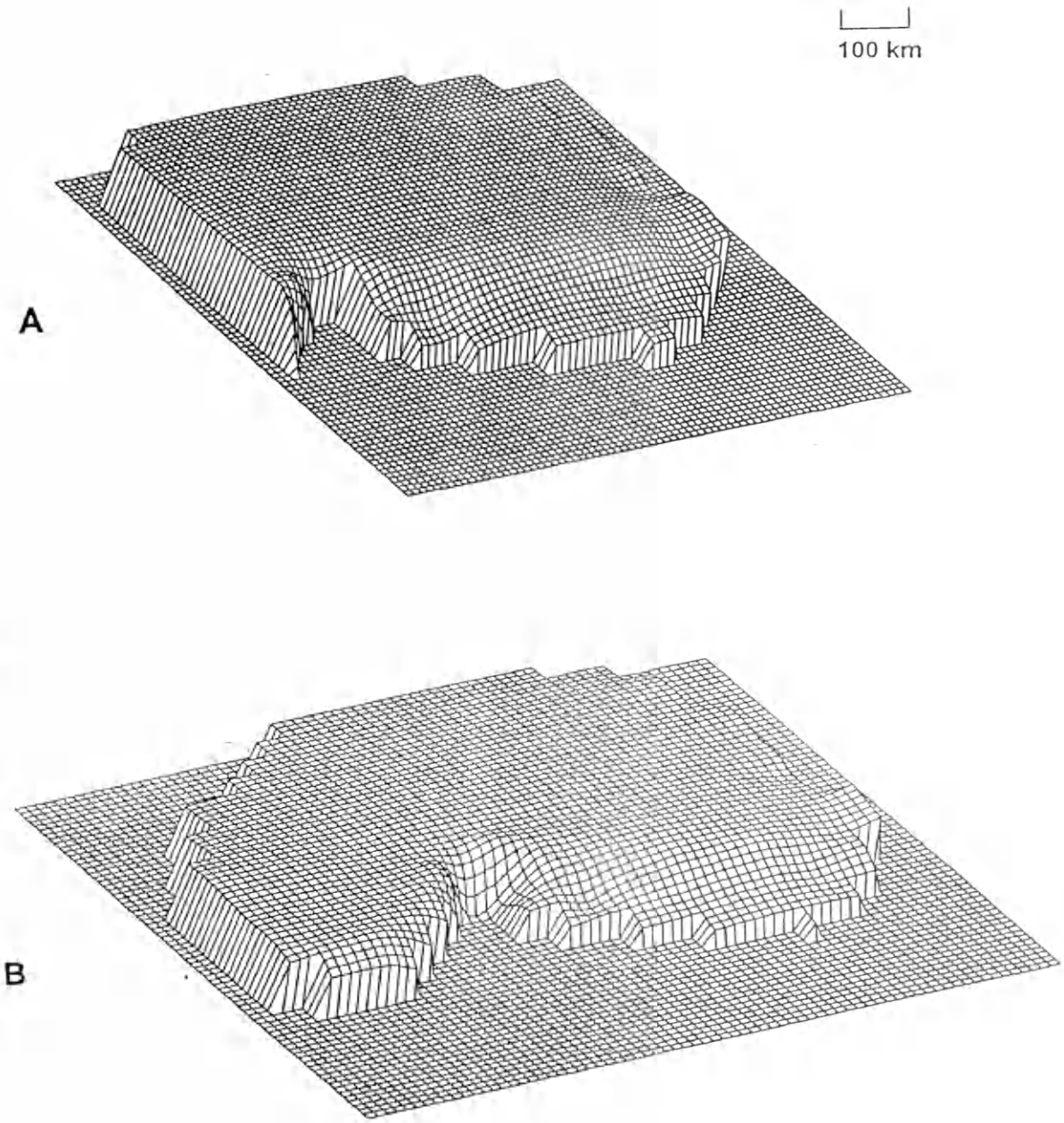

Figure 21 - A. Plot of SURFER™ surface used for volume calculations.
A: Marine portion bounded in the west by the Swatch of No Ground.
B: Marine portion bounded in the west by Hugli River.

terrestrial, the area seaward of the modern coastline is considered marine .

Budget Estimates

Based on the estimated annual sediment load of 1060 x 10^6 t/y (Milliman and Syvitski, 1992), the volume of marine material (integrated over 7,000 years and assuming a sediment density of 1.1g/cc) on the shelf, with a western boundary at the Swatch of No Ground, is an estimated 27% of the total input . The terrestrial component to this same boundary is 3.6%. Taking the western boundary to be the mouth of the Hugli river, the marine portion accounts for 31%, and the corresponding terrestrial portion, 4.2%. Although sediment appears to be channeling through the Swatch, as evidenced by mass movements and relatively high sedimentation rates, the Hugli probably represents a more accurate western boundary because of its role in the past as a major outlet for the river.

Error for these budget estimates likely is large as they are based on a current total load that may not be valid for the entire Late Holocene. Man-made effects, such as farming, can increase the load that the river carries, whereas man-made river control such as dams can lessen the load by trapping sediment and preventing it from continuing down stream. The ages that are taken from

Umitsu provide further room for error, and other, although smaller, rivers also debouch onto the shelf in this area they are ignored in the budget. Most importantly, the boundaries were based on sedimentary facies and morphological characteristics, and are as such, arbitrary to some degree.

An important consideration is that the measurements of load are taken some distance upstream of the coastline. A 1990 UNESCO report suggests that the amount reaching the coastline may be only 5×10^8 tons/years, only half of the measured total load. In that case, the amount of sediment accumulating on the shelf could be as high as 55% of what actually reaches the coastline. Because the load may be diminished by accommodation on the flood plain, diversion of river water, and damming, it is likely that the measured load of the river differs greatly from what debouches from the mouths. More detailed study is necessary to ascertain the role of the delta plain in the overall budget.

The Ganges-Brahmaputra and Other Analogous Systems: A Comparison

The Amazon, Huanghe and Ganges-Brahmaputra-Meghna Rivers are similar in terms of sediment discharge, with estimated loads of 1200×10^6, 1100×10^6 and 1000×10^6 t/y, respectively (Milliman and Syvitski, 1992) . The rivers enter energetic marine settings and both the Amazon and Huanghe have been

found to form subaqueous deltas (Nittrouer et al., 1986; Alexander et al., 1990). Ancient deposits from the North American Cretaceous, such as the Tropic Shale and Tunuk Member of the Mancos Shale in southern Utah (Leithold, 1993), and Lower Cody Shale of the southeastern Big Horn Basin in Wyoming (Asquith, 1970) are thought to be good analogues for subaqueous deltas. Key characteristics of these modern and ancient environments are shown in table 2 and discussed in the following sections.

Modern Systems

The Amazon River empties onto a pericontinental sea on the continental margin off Northern Brazil (Fig. 22). Sediment transported by the Amazon is primarily derived from tributaries draining the Andes mountain chain (Gibbs, 1967). Peak water discharge displays some seasonal variations with highest rates observed during May-June (Nittrouer et al., 1991). The peak sediment discharge precedes the water peak by about 1 month (Meade et al., 1985). The oceanographic regime is characterized by strong tidal and coastal currents with moderate wave activity. Intense reworking of sediments on the inner shelf prevent Amazon sediments from depositing permanently (Kineke et al, 1991). The Amazon River plume extends offshore over the wide shelf for more than 300

			Modern	Analogues	Ancient	Analogues
sub-environment		Ganges-Brahmaputa River 1069 x 10^6 t/y	Amazon River[1,4] 1200 x 10^6 t/y[2]	Huanghe River[3] (subaqueous portion in Yellow Sea) 1100 x 10^6 t/y[2]	Cody Shale[5]	Tropic Shale[6] and Tunuk Member of the Mancos Shale
Topset beds	*water depth*	15-25 m	10-30m	2-12 m	NA	NA
	slope	.04°	.02°	.2-.3°	gentle	gentle
	sediment accumulation rate	1.9 cm/yr	≤1 cm\yr	1-2 mm/yr	repredents 30-40% of formation	relatively low sedimentation rates
	sedimentary structure	inter-laminated silts and mud	parallel-bedded acoustic reflectors	undisturbed, parallel-bedded sediments	bioturbated	biorturbated
	grain size	mud and silt	silt/clay with sandy interbeds	coarse to medium silts	shale	sandy-mudstone, silty-musdtone
Foreset beds	*water depth*	25-60 m	40-60 m	10-14 m	NA	NA
	slope	.19°	.05°-.57°	.2°-.5°	up to .5°	.13°
	sediment accumulation rate	5.5-12.1 cm/yr	10 cm/yr	4-6 mm/yr	represents 50-60% of deposit	NA
	sedimentary structures	well stratified, progressively thickening muds	stratified muds over basal transgressive sand surface	shallow, well sratified channel cuts	very well laminated	laminated strata
	grain size	muds	muds	NA	shale	silty-mudstone
Bottomset beds	*water depth*	60-80 m	60-100 m	14-100 m	NA	NA
	slope	.022°	.03°	nearly flat	NA	NA
	sediment accumulation rate	0.3 cm/yr	.3 cm/yr	2-3 mm/yr	represents 10% of sediment	NA
	sedimentary structures	stratified	stratified	stratified	bioturbated	laminated with some bioturbation
	grain size	muds	sands	NA	shale	clay-stone

Table 2 - Comparison of Ganges-Brahmaputra River System with modern (Amazon and Huanghe) and ancient analogues (Cody and Mancos Shales).
[1]Nittrouer et al., 1986; [2]Milliman and Syvitski, 1992; [3]Alexander et al., 1991; [4]Kuehl el al., 1986; [5]Asquith, 1970; [6]Leithold, 1993.

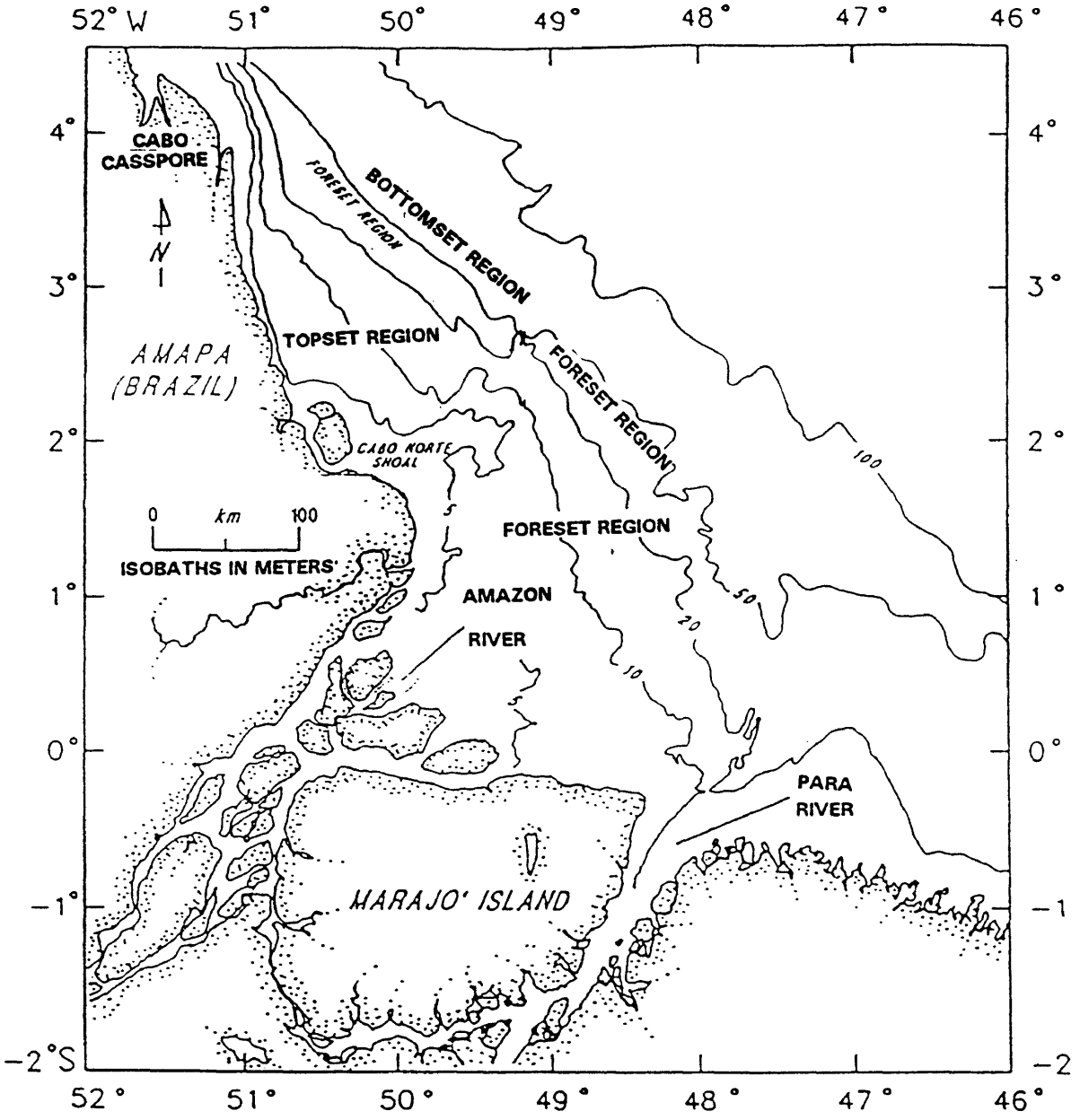

Figure 22 - Bathymetric chart of the Amazon shelf showing approximate locations of topset, foreset and bottomset regions of the subaqueous delta.

km and nearly 1,000 m northwest entrained by the North Brazil Current (Geyer et al., 1991). The subaqueous delta displays characteristic gently sloping topset beds, steeply sloping foreset beds and gently sloping bottomset beds (Kuehl et al., 1986) prograding over a transgressive sand layer (Nittrouer et al., 1986). Topsets beds display parallel bedding with evidence of bioturbation, foreset beds are stratified muds over a basal transgressive sand layer and bottomset beds are stratified with bioturbation. Nittrouer et al. (in press) summarize the current research on the Amazon shelf. Muddy sediment from the Amazon River is transported northwest of the river mouth on short time scales (tens of years). Some of the sediment moves seaward and rapidly accumulates on the foreset beds. Some moves northwestward and causes progradation of the northernmost Amapa shoreline. Strong tidal currents cause the southern Amapa shoreline to undergo erosion today. Roughly half of the discharge of the Amazon is accommodated on the adjacent shelf when averaged over time scales of decades-centuries (Kuehl et al.,1986). About one sixth of the load is accommodated by accretion on the Amapa shoreline and by north western bypassing of sediments. It is proposed that the remaining portion of the overall load is accommodated in the flood plain (Nittrouer et al., in press).

The Huanghe River delivers sediment to the Gulf of Bohai and ultimately

to the relatively shallow epicontinental Yellow Sea (everywhere <100m). Although water discharge of the Huanghe is two orders of magnitude lower than the Amazon and Ganges-Brahmaputra, sediment load is comparable (Milliman and Syvitski, 1992). This large sediment load of silt eroded from the loess plateau of interior China creates a negatively buoyant plume with the highest loads entering the Gulf during the summer monsoon period between July-October (Wright and Nittrouer, in press). The dry winter monsoon (December-February) is a period of low precipitation and low discharge, which coincides with high wave activity and strong winds. About 90% of the sediments discharged from the Huanghe remain within 30 km of the mouth (Wright and Nittrouer, in press). This large influx of sediments has resulted in rapid growth of the subaerial delta which advances between 0.5 and 1.0 km/y (Ren and Shi, 1986; Yang and Lu, 1987). An estimated 10-15% of Huanghe sediment escapes the Gulf of Bohai and is forming a subaqueous delta in the Yellow Sea (Bornhold et al., 1986; Prior et al., 1986) (Fig. 23). Topset beds are characterized by undisturbed, parallel bedding. Foreset beds display shallow, well stratified channels and bottomset beds are stratified. The oceanographic regime is characterized by strong tidal currents and waves (Alexander et al.,1991). Most of the Huanghe subaqueous delta consists of fine sediments (7-8ϕ) and

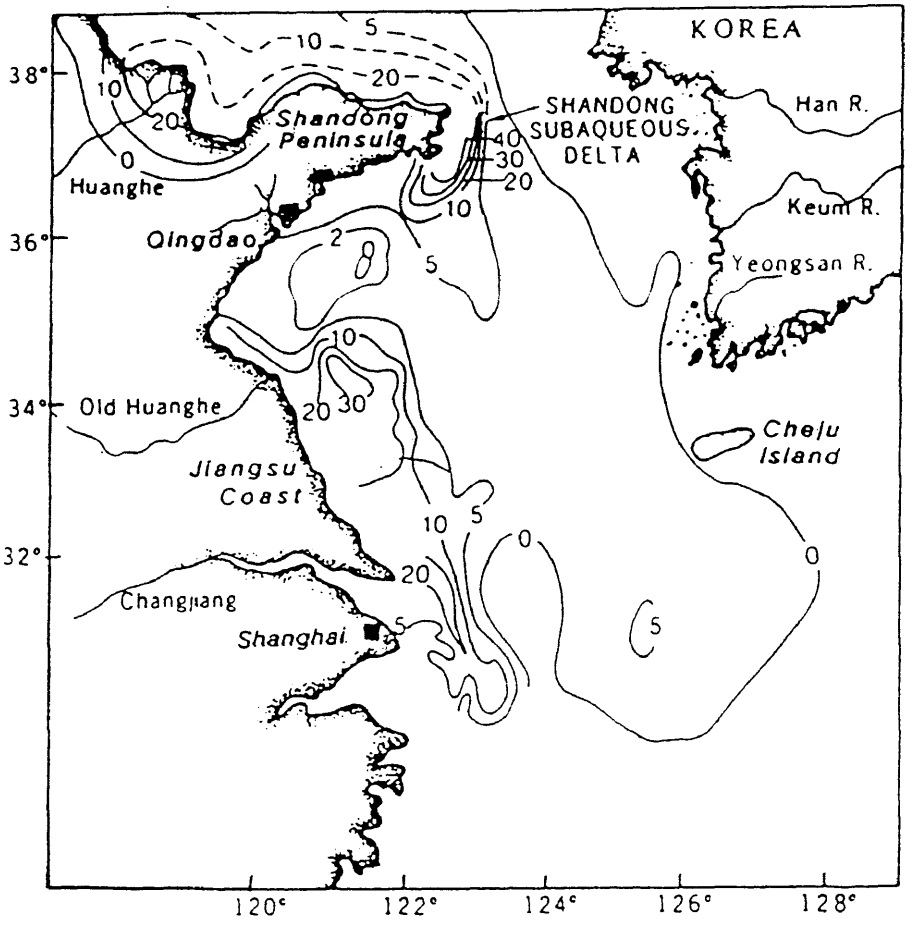

Figure 23 - The Yellow Sea and the Huanghe subaqueous delta, contours depict approximate Holocene sediment thickness (from Milliman, 1987).

sedimentation extends over the entire 800 km length of the Yellow Sea (Alexander et al., 1991).

All three systems display the distinctive morphology of subaqueous deltas: the relative gradients of the respective deltas are similar displaying gently sloping topsets, more steeply dipping foresets and gentle bottomsets with the corresponding relative sedimentation rates. (see table 2). Highest sedimentation rates are found in the foreset region. The Amazon has the highest foreset sedimentation rates (>30 cm/y), followed by the Ganges-Brahmaputra (<12 cm/y) and the subaqueous portion of the Huanghe (<6 mm/y).

Except for the Huanghe, the subaqueous deltas are forming in waters of similar depths (up to about 100m) in similar oceanographic settings. The bulk of the Huanghe subaqueous delta is forming in relatively shallow water, between 2 and 12 m water depths. Whereas the Ganges-Brahmaputra deposits are more areally restricted on the shelf (although evidence suggests some bypassing of sediments to the Bengal Fan via the Swatch of No Ground), the Huanghe deposits extend over the 800 km length of the Yellow Sea (Alexander et al., 1991) and the Amazon extends nearly 1600 km to the northwest (Kuehl et al, 1986). The timing of water and sediment discharge and high energy oceanographic conditions plays an important role in the nature of sediment

dispersal for the rivers. In the case of the Amazon and Ganges-Brahmaputra, highest sediment discharge is in phase with maximum marine energy causing resuspension and deposition away from the river mouths. In contrast, the period of highest sediment and water discharge from the Huanghe is during the time of lowest marine energy in the Gulf of Bohai. This time lag allows sediments to partially consolidate and resist resuspension when subjected to higher energy conditions resulting in accumulation of up to 90% of the sediments within 30 km of the river mouth. Only about 10-15% is transported farther along the dispersal system to the subaqueous portion of the delta in the Yellow Sea, presumably during the winter monsoon (Wright and Nittrouer, in press).

The stratigraphy of the near shore region of the Ganges-Brahmaputra subaqueous delta is obscured on the seismic profiles mainly due to high sand content. In contrast to the relatively fine grained sediment comprising the Amazon and Huanghe subaqueous deltas (averages of 7-8ϕ) , the Ganges-Brahmaputra is coarser (averages of 5-9ϕ) and is characterized predominantly by sand near the river mouth. In contrast to the Ganges-Brahmaputra, widespread methane gas deposits are present on the inner Amazon shelf. Gas deposits appear to be locked beneath impermeable layers, typically old erosional mud layers, and preclude high-resolution seismic studies in this region

(Figueiredo and Nittrouer, in press). Geochemical analysis of gas deposits from cores reveal a relatively recent biogenic origin (Nittrouer et al., in press)

The Ganges-Brahmaputra, Amazon and Huanghe subaqueous deltas all display underlying erosional surfaces. Cut and fill structures suggest relict gullies and channels from times of lowered sea level. Cut and fill structures are interpreted to represent previous subaerially exposed surfaces later in filled with advancing sediment. Marine landslides, slumping and faulting contribute to movement of sediment from the site of initial deposition (Wright et al., 1990) and attest to the active nature of shelf sedimentation in areas which this occurs. Mass movement is seen around the Swatch of No Ground on the Bengal Shelf which is an areas of high sedimentation rates (6 -12 cm/y). In contrast to the Ganges-Brahmaputra and Huanghe, these structures are rare on the Amazon shelf.

Ancient Analogues

The Cody Shale of the southeastern Bighorn Basin in Wyoming (Fig. 24) is an ancient example of a subaqueous delta, exhibiting the clinoform stratigraphy of its modern analogues. Sediments are thin in the topset region (30-40% of total volume of sediment comprising the deposit) where evidence of

A

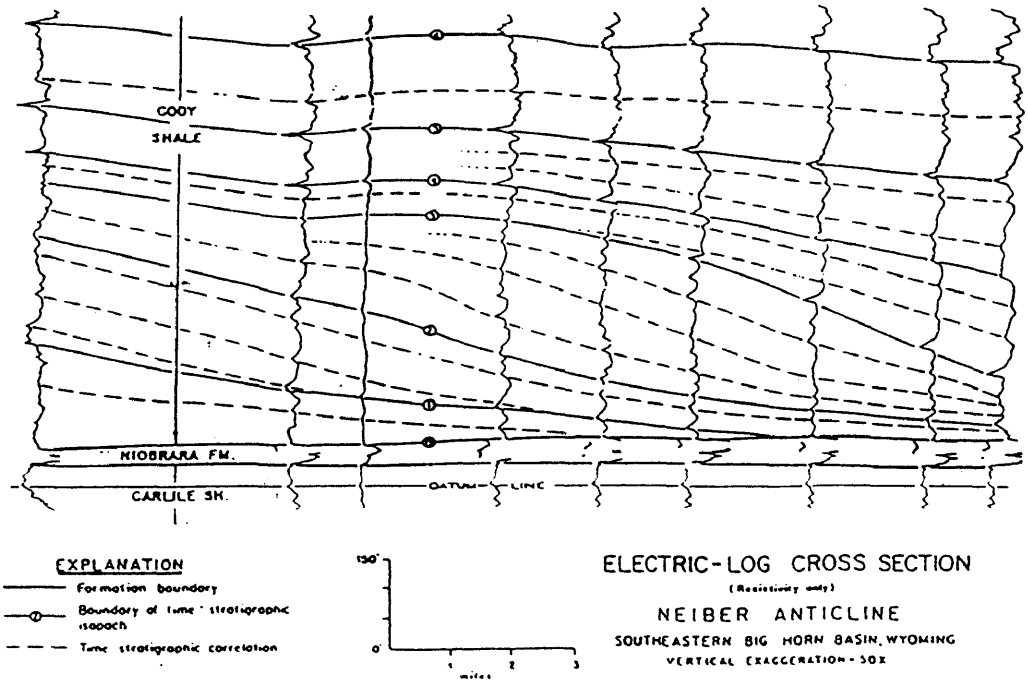

B

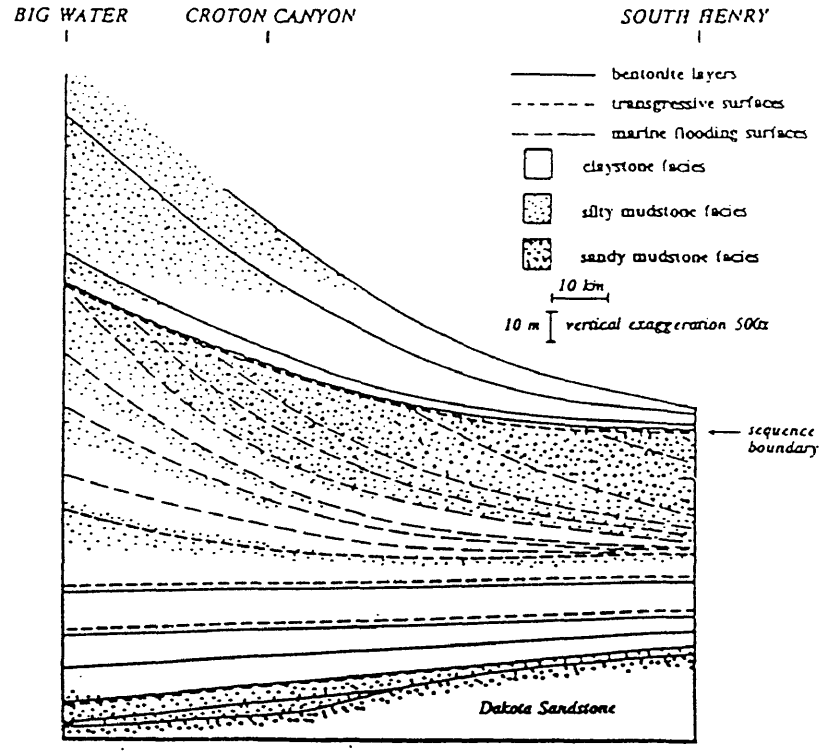

Figure 24 - A. Cody Shale, Southeastern Big Horn Basin, taken from Asquith, 1970. B. Tropic Shale and Tunuk Member of the Mancos Shale in Souther Utah (from Leithold, 1994).

bioturbation is present. The thicker foreset beds (50-60% of the sediment deposit) steepen considerably. The amount of sediment accumulated on the shelf is primarily a function of subsidence. The well-laminated beds are the result of increased sedimentation rates while the thin, "starved," bottomset beds once again exhibit bioturbation (Asquith, 1970).

The Tropic Shale and Tunuk Member of the Mancos Shale of Southern Utah (Fig. 24) also have clinoform structure with corresponding bioturbation in areas of low sediment accumulation and physical lamination in areas of high accumulation. Topset beds have relatively low sedimentation rates and display evidence of bioturbation (Leithold, 1993). Foreset beds have distinct laminations, thought to be caused by increased sedimentation rates. The bottomset beds have the most distinct lamination, but it is believed that this lamination is due to anoxic conditions precluding habitation by benthic organisms

Modern vs. Ancient Subaqueous Deltas

The subaqueous delta of the Ganges-Brahmaputra and its modern and ancient analogues have similar structural features. All have the characteristic clinoform stratigraphy of gently sloping topset beds with correspondingly low

sedimentation rates, which grade into more steeply dipping foreset beds with higher accumulation rates and finally, the foresets lap onto gently sloping bottomsets beds with very low sedimentation rates. This differentiation in sedimentation rates causes aggradation and progradation of the subaqueous delta. All the systems have some evidence of previous transgressive surfaces underlying the deltas.

In areas with little biological disturbance, laminated sediments are common for both modern and ancient settings. Because of low sedimentation rates, the outer foreset and bottomset regions often are bioturbated. Rapid sedimentation, such as in the inner foreset region, inhibits benthic community developement probably because of high levels of turbidity and sediment instability produced by the influx of sediment. For all the examples of subaqueous deltas, the foreset region exhibits physically laminated muds. Evidence of mass movement and penecontemporaneous deformation are characteristic of both modern and ancient deltas (Nittrouer et al., 1986; Alexander et al., 1991), most likely caused by rapid accumulation of sediments. Similarities between sediment wedges forming seaward of rivers which enter energetic marine environments are seen between three of the largest modern rivers, as well as important sequences of the rock record. While potions of each

delta may be classified as subaqueous, each has stratigraphy unique to its own environment.

Conclusions

1. Seismic reflection profiles of the sediment wedge seaward of the Ganges-Brahmaputra river system reveals clinoform stratigraphy characteristic of a subaqueous delta. Radioisotope profiles show relatively low sedimentation rates in the inner topset region, with increasing rates toward the seaward extent of the topset beds and inner foreset beds. Outer foresets beds reveal relatively low accumulation rates and decreasing rates on the bottomset beds. These relations are reflected in the nature of the seismic profiles. Reflectors in the outer topset region diverge due to increased sedimentation rates, while the foreset beds converge due to lower sedimentation rates.

2. Grain size distribution, sediment accumulation rates and sand wave asymmetry suggest sediment transport is predominantly south and westward. Grain size shows a fining toward the west and the south, with the finest fractions found near the submarine canyon, Swatch of No Ground, which incises the western shelf. Sedimentation rates are highest in the western portion of the subaqueous delta near the Swatch of No Ground (5.5 - 12.1 cm/y). Sand waves found near the eastern coast of Chittagong are oriented with their stoss side facing east.

3. Evidence of mass movement, and high sedimentation rates suggest modern sediment is being channeled off-shelf to the Bengal Fan via the Swatch of No Ground. Seismic profiles near the head of the canyon show slumps and growth faults, and irregular sediment surfaces indicating penecontemporaneous deformation associated with high sedimentation rates. This area boasts the highest sedimentation rates found on the subaqueous delta (6 -12 cm/y).

4. Volume determination using SURFER™ reveal the subaqueous delta accommodates about 30% of the sediment load carried by the combined river system during the Late Holocene. The flood plain and off-shelf transport accommodate the remainder.

5. The subaqueous delta of the Ganges-Brahmaputra is similar to other modern subaqueous deltas forming off other large river systems entering energetic marine settings as well as key formations in the geologic record. These similarities suggest this is an important mode of delta growth for the world's largest rivers.

Appendix A - Gamma Spectroscopy

Core	DEPTH IN CORE (midpt.)	LEAD-210 TOTAL ACTIVITY (dpm/g)	LEAD-210 EXCESS ACTIVITY (dpm/g)	LEAD-210 ERROR (dpm/g)	THORIUM-234 EXCESS ACTIVITY (dpm/g)	THORIUM-234 ERROR (dpm/g)	CESIUM-137 TOTAL ACTIVITY (DPM/G)*100	CESIUM-137 ERROR (DPM/G)*100	RADIUM-228/ RADIUM-226 ACTIVITY RATIO	RADIUM-228/ RADIUM-226 ACTIVITY RATIO ERROR
1	1	14.18	12.75	0.08			21.81	3.78	1.22	0.14
	11	5.20	3.78	0.09			14.70	3.13	1.29	0.23
	11	4.95	3.49	0.06			10.46	2.22	1.28	0.11
	21	1.64	0.45	0.05			0.00	0.00	1.43	0.13
	31	1.48	0.28	0.05			0.00	0.00	1.30	0.11
	41	1.62	0.43	0.06			0.00	0.00	1.45	0.15
	51	1.53	0.29	0.06			0.00	0.00	1.37	0.14
	61	1.46	0.13	0.06			0.00	0.00	1.28	0.12
	71	1.48	0.24	0.07			0.00	0.00	1.35	0.19
	81	1.68	0.34	0.06			0.00	0.00	1.30	0.12
4	1	8.28	5.65	0.09	1.10	0.56	26.48	3.02	1.10	0.08
	3	7.85	5.43	0.09	1.19	0.49	24.71	2.38	1.16	0.11
	5	8.16	5.76	0.13	0.04	0.54	35.65	3.61	1.12	0.13
	7	10.40	7.94	0.05			13.56	1.44	1.09	0.05
	9	12.49	10.09	0.10			28.38	3.26	0.99	0.10
	11	11.39	9.00	0.09			22.61	2.40	1.19	0.09
	16	6.94	4.56	0.07			17.41	2.40	1.33	0.08
	21	6.53	3.94	0.12			21.01	4.02	1.26	0.13
	26	6.98	4.68	0.09			0.00	0.00	1.36	0.11
	31	5.63	3.35	0.08			0.00	0.00	1.51	0.10
	36	3.21	0.80	0.07			0.00	0.00	1.27	0.08
	41	2.86	0.45	0.08			0.00	0.00	1.22	0.08
	46	3.27	0.85	0.06			0.00	0.00	1.34	0.08
	51	4.02	1.60	0.11			0.00	0.00	1.34	0.12
	56	3.18	0.79	0.08			0.00	0.00	1.36	0.12
	61	2.89	0.34	0.08			0.00	0.00	1.35	0.09
	65	2.96	0.89	0.08			0.00	0.00	1.54	0.11
	71	3.01	0.54	0.09			0.00	0.00	1.48	0.11
	76	2.75	0.40	0.06			0.00	0.00	1.41	0.08
	81	2.65	0.38	0.07			0.00	0.00	1.44	0.10
	86	2.63	0.42	0.07			0.00	0.00	1.56	0.09
	91	2.61	0.34	0.08			0.00	0.00	1.36	0.11
	96	2.53	0.28	0.20			0.00	0.00	1.34	0.18
	101	2.57	0.29	0.06			0.00	0.00	1.24	0.08
	111	2.55	0.26	0.07			0.00	0.00	1.53	0.11
	121	2.86	0.40	0.09			0.00	0.00	1.37	0.11
	131	2.96	0.65	0.07			0.00	0.00	1.53	0.12
	141	2.73	0.39	0.09			0.00	0.00	1.47	0.11
	141	2.82	0.41	0.08			0.00	0.00	1.46	0.11
	151	2.70	0.31	0.08			0.00	0.00	1.40	0.09

Core	DEPTH IN CORE (midpt.)	LEAD-210 TOTAL ACTIVITY (dpm/g)	LEAD-210 EXCESS ACTIVITY (dpm/g)	LEAD-210 ERROR (dpm/g)	THORIUM-234 EXCESS ACTIVITY (dpm/g)	THORIUM-234 ERROR (dpm/g)	CESIUM-137 TOTAL ACTIVITY (DPM/G)*100	CESIUM-137 ERROR (DPM/G)*100	RADIUM-228/ RADIUM-226 ACTIVITY RATIO	RADIUM-228/ RADIUM-226 ERROR
5	41	4.67	2.03	0.10			15.97	2.40	1.10	0.10
	61	7.04	4.65	0.08			19.31	2.74	1.12	0.09
	61	7.44	4.93	0.08			21.31	2.34	1.14	0.09
	66	5.46	2.83	0.10			25.28	2.35	1.09	0.09
	71	4.55	1.89	0.08			18.16	1.99	1.15	0.08
	76	5.10	2.67	0.07			23.14	2.00	1.26	0.09
	81	6.97	4.41	0.11			18.85	2.79	1.21	0.10
	91	6.27	3.58	0.09			20.10	3.09	1.13	0.08
	96	6.03	3.43	0.09			22.48	3.16	1.09	0.09
	101	5.68	3.15	0.11			25.81	3.46	1.13	0.09
	111	4.34	1.77	0.09			24.19	3.06	1.33	0.11
	121	6.17	3.60	0.10			21.02	2.41	1.26	0.10
	131	4.54	1.96	0.09			21.16	2.70	1.28	0.09
	141	5.87	3.35	0.06			21.45	1.99	1.31	0.06
	151	5.27	2.70	0.09			25.05	3.04	1.34	0.10
	161	6.04	3.43	0.09			21.53	2.69	1.31	0.09
	171	5.28	2.69	0.08			19.33	1.88	1.26	0.08
	181	5.35	2.84	0.08			22.62	2.58	1.27	0.08
	191	4.60	2.02	0.10			26.67	3.39	1.26	0.09
8	1	5.05	2.73	0.07	1.19	0.54	11.31	1.55	1.07	0.07
	3	5.73	3.34	0.08	-0.50	0.47	16.48	2.31	1.03	0.07
	5	5.50	3.04	0.10	-0.10	0.55	21.91	2.83	1.03	0.09
	7	5.36	2.74	0.08	0.03	0.55	12.46	2.34	0.95	0.07
	9	5.07	2.52	0.08	-0.47	0.43	12.71	2.47	1.15	0.08
	11	4.81	2.28	0.05			0.00	0.00	1.12	0.05
	16	3.47	1.39	0.06			13.07	2.47	1.11	0.11
	21	3.98	1.45	0.07			9.27	1.96	1.15	0.08
	26	4.36	1.82	0.07			12.54	1.73	1.09	0.07
	31	4.67	2.20	0.08			13.71	2.13	1.14	0.08

Core	DEPTH IN CORE	LEAD-210 TOTAL ACTIVITY	LEAD-210 * EXCESS ACTIVITY	ERROR	THORIUM-234 EXCESS ACTIVITY	ERROR	CESIUM-137 TOTAL ACTIVITY	ERROR	RADIUM-228/ RADIUM-226 ACTIVITY RATIO	ERROR
	(midpt.)	(dpm/g)	(dpm/g)	(dpm/g)	(dpm/g)	(dpm/g)	(DPM/G)*100	(DPM/G)*100		
9	16	4.43	1.95	0.07			12.57	1.74	1.10	0.08
	21	3.82	1.48	0.05			12.28	1.44	1.15	0.07
	26	4.43	2.18	0.09			12.72	1.98	1.20	0.10
	31	3.09	1.18	0.04			8.07	0.77	1.08	0.06
	36	3.27	1.28	0.06			0.00	0.00	1.15	0.08
	41	3.34	1.33	0.06			11.78	1.41	1.16	0.08
	46	3.10	1.37	0.05			10.02	1.29	1.11	0.08
	51	4.04	1.94	0.07			12.27	2.44	1.22	0.10
	56	4.19	1.68	0.08			13.50	2.08	1.14	0.08
	61	4.56	2.22	0.08			0.00	0.00	1.09	0.08
	66	4.41	1.89	0.08			19.19	2.22	1.04	0.08

* Excess activities are calculated by subtracting Ra-226 from total Pb-210 activities. Intervals with calculated values below 0.5 dpm/s are considered to have no signifigant excess activity as about a 0.5 dpm offset in supported Pb-210 and Ra-226 measurements is observed.

Appendix B- Formulas for sediment accumulation rates using radioisotopes

^{210}Pb

$$a = \lambda Dx / \ln (A/Ao) \qquad \lambda = \ln 2 / t_{1/2}$$

Where a= accuulation rate, D_x= depth in seabed (cm), A_0=intial activity at time t=0, A=observed activty, t= time in years, λ=decay constant for ^{210}Pb (22.3/y), and $t_{1/2}$=half-life, .

^{137}Cs

$$a = \frac{\text{depth of maximum sea bed penetration}}{\text{time frame for existence of Cs in the Atmophere, 35 years}}$$

^{228}Ra / ^{226}Ra ratios

$$\ln (1-((^{228}Ra/^{226}Ra) / (^{232}Th/^{226}Ra))) / d = -\lambda / a$$

Where a=accumulation rate, d = depth in core and λ is ln 2/ $t_{1/2}$. $^{228}Ra/^{226}Ra$= the measured activty ratio, $^{232}Th/^{226}Ra$ = calculated activity ratio, λ= decay constant for ^{228}Ra (0.121/y), d= depth in seabed (cm), a= sediment accumulation rate(cm/y) and t= time in years.

Appendix C - ^{137}Cs profiles for all cores

Core 1

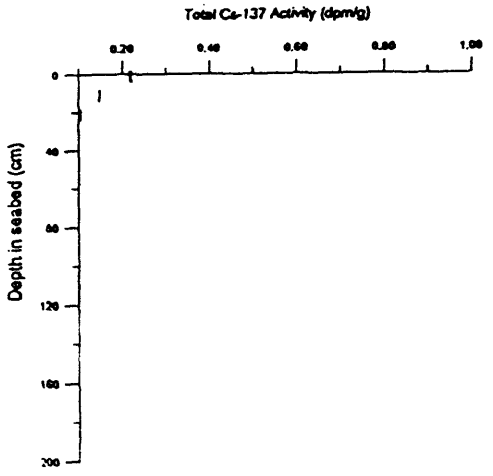

Core 4

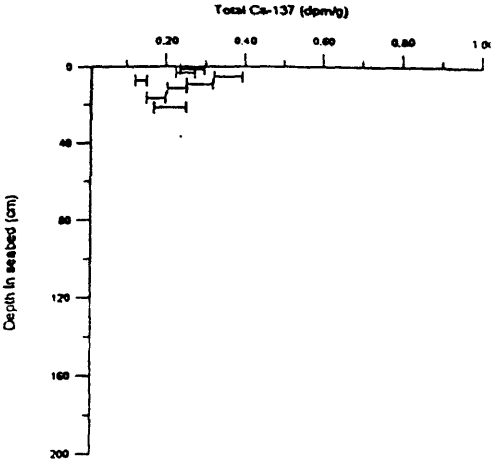

Core 5

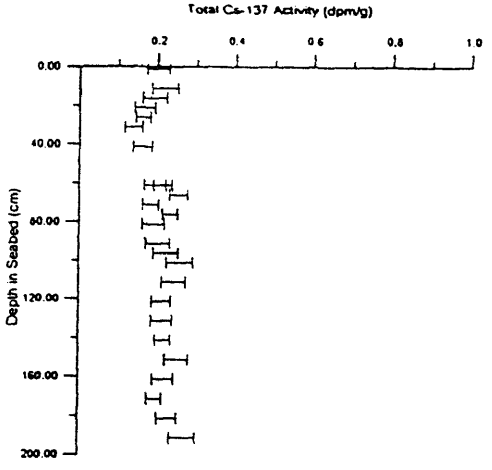

Core 6

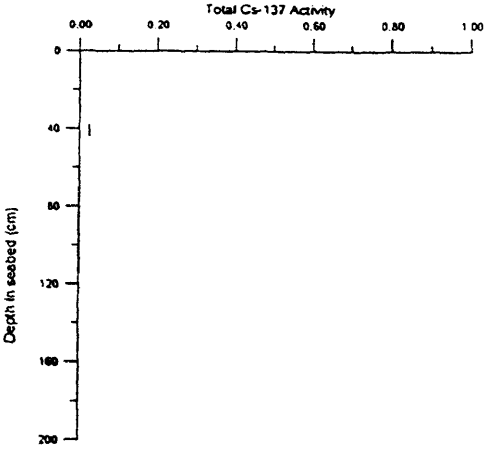

Core 8

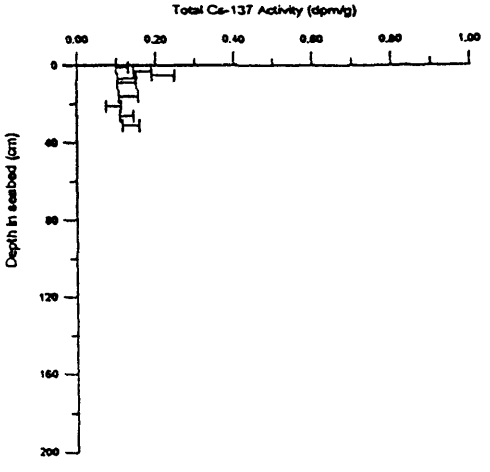

Core 9

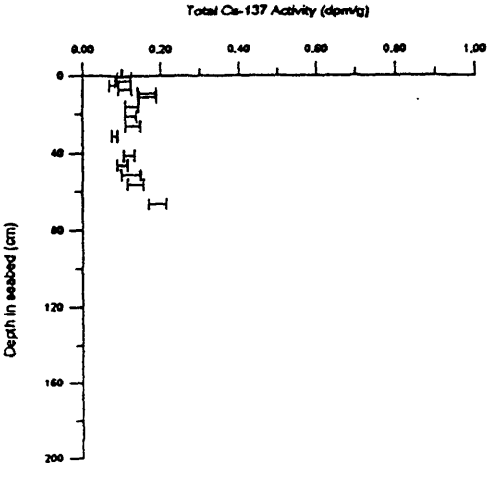

Appendix D - ^{210}Pb profiles for all cores

Core 1

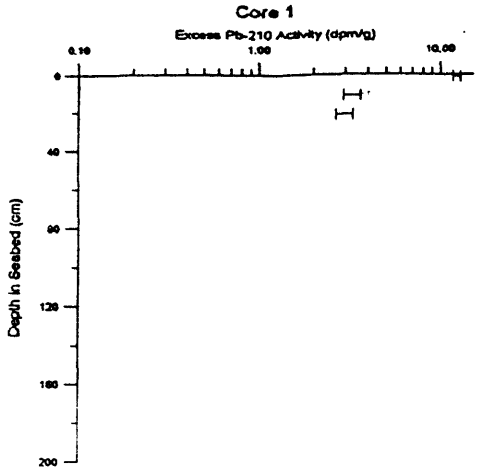

Core 4

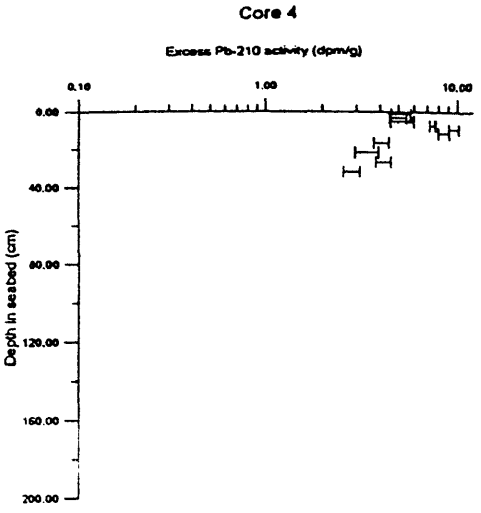

Core 5

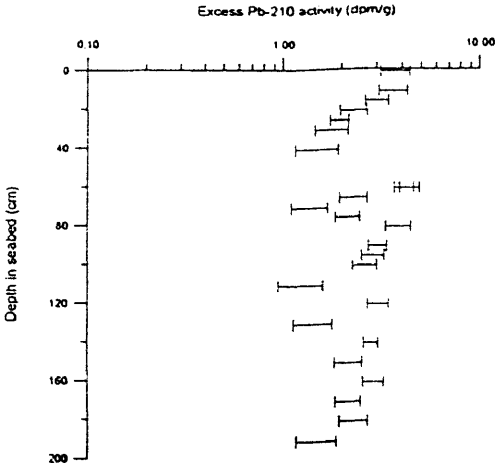

Core 6

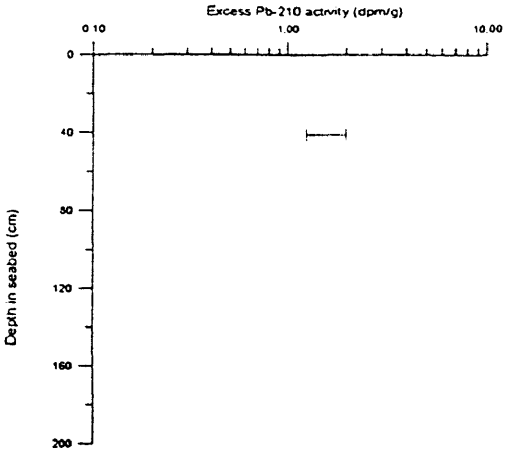

Core 8

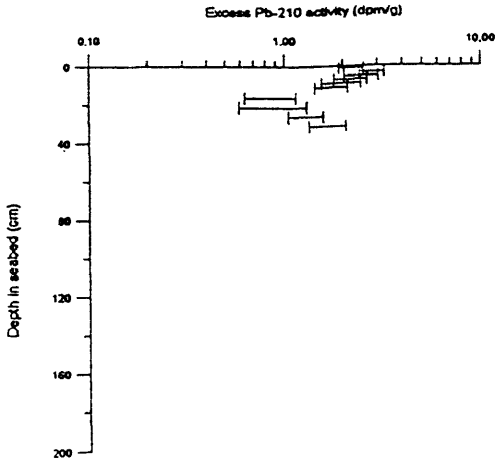

Core 9

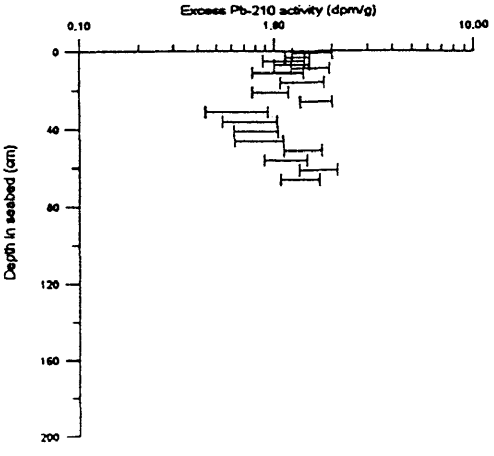

Appendix E - Bangladesh Sedigraph Grain-Size Data 1991

Sample	Mean Depth (cm)	Mean Grain Size (phi)	Average Mean for Core	Sorting
Core 1				
A911-0	1.0	6.9	7.9	3.5
A911-20	21.0	8.1		2.4
A911-30	31.0	6.5		4.0
A911-80	81.0	7.6		2.4
A911-100	101.0	8.7		2.6
A911-140	141.0	9.5		2.6
Core 4				
A914-8	9.0	6.9	8.5	2.1
A914-15	16.0	9.8		1.8
A914-25	26.0	8.4		2.5
A914-55	56.0	8.2		2.2
A914-85	86.0	8.4		2.1
A914-90	91.0	8.3		2.5
A914-140	141.0	9.1		2.3
A914-160	161.0	8.8		2.4
A914-200	201.0	8.2		2.7
Core 5				
A915-0	1.0	8.7	8.5	2.0
A915-20	21.0	9.4		2.2
A915-25	26.0	7.4		2.4
A915-40	41.0	8.1		2.3
A915-75	76.0	8.7		2.1
A915-100	101.0	9.0		2.1
A915-130	131.0	8.0		1.7
A915-140	141.0	8.7		2.2
Core 6				
A916-0	1.0	7.9	7.9	2.4
Core 8				
A918-0	1.0	7.0	7.0	1.9
A918-8	9.0	7.0		2.4
A918-15	16.0	6.9		2.3
A918-25	26.0	6.9		2.3
Core 9				
A919-0	1.0	8.6	7.6	3.3
A919-2	3.0	7.4		2.1
A919-10	11.0	9.0		0.7
A919-15	16.0	8.4		1.2
A919-45	46.0	5.6		2.6
A919-50	51.0	6.7		2.7

Appendix - F Sesimic Navigation Data

Seismic Line #	Time Interval	# Minutes	Distance (km)	km/minute	Corrected Dist. / T (km/min.)	Total Dist. (km)
A	0710-0845	95.00	15.70	0.17	0.17	16.00
	0845-0900	15.00	3.30	0.22	0.19	2.78
	0900-1000	60.00	6.60	0.11	0.17	9.91
	1000-1015	15.00	4.80	0.32	0.22	3.25
	1015-1030	15.00	1.50	0.10	0.18	2.65
	1030-1045	15.00	4.60	0.31	0.24	3.63
	1045-1100	15.00	2.00	0.13	0.18	2.70
	1100-1115	15.00	5.40	0.36	0.27	4.00
	1115-1130	15.00	2.60	0.17	0.22	3.33
	1130-1145	15.00	4.80	0.32	0.28	4.27
	1145-1200	15.00	5.50	0.37	0.29	4.30
	1200-1218	18.00	5.50	0.31	0.33	5.95
	1218-1230	12.00	2.80	0.23	0.30	3.62
	1230-1300	30.00	15.20	0.51	0.35	10.46
	1300-1315	15.00	3.90	0.26	0.33	5.00
	1315-1320	5.00	2.60	0.52	0.43	2.14
					Total Dist. (km)	*83.99*

Seismic Line #	Time Interval	# Minutes	Distance (km)	km/minute	Corrected Dist. / T (km/min.)	Total Dist. (km)
B	1905-1915	10.00	2.20	0.22	0.22	2.20
	1915-1930	15.00	3.10	0.21	0.22	3.23
	1930-1945	15.00	3.10	0.21	0.21	3.17
	1945-2000	15.00	3.30	0.22	0.21	3.17
	2000-2015	15.00	3.10	0.21	0.21	3.17
	2015-2046	16.00	6.50	0.41	0.28	4.44
	2046-2100	14.00	2.20	0.16	0.26	3.59
	2100-2115	15.00	3.50	0.23	0.27	3.98
	2115-2130	15.00	3.50	0.23	0.21	3.12
	2130-2146	16.00	3.30	0.21	0.22	3.59
					Total Dist. (km)	*33.66*

Seismic Line #	Time Interval	# Minutes	Distance (km)	km/minute	Corrected Dist. / T (km/min.)	Total Dist. (km)
C	0920-0931	11.00	3.10	0.28	0.28	3.09
	0931-0945	14.00	2.40	0.17	0.24	3.42
	0945-1000	15.00	2.40	0.16	0.20	3.07
	1000-1015	15.00	2.40	0.16	0.16	2.46
	1015-1030	15.00	2.60	0.17	0.16	2.47
	1030-1045	15.00	5.00	0.33	0.22	3.33
	1045-1100	15.00	6.60	0.44	0.32	4.73
	1100-1115	15.00	2.60	0.17	0.32	4.73
	1115-1130	15.00	2.60	0.17	0.26	3.93
	1130-1145	15.00	4.10	0.27	0.21	3.10
	1145-1200	15.00	2.90	0.19	0.21	3.20
					Total Dist. (km)	*37.53*

Seismic Line #	Time Interval	# Minutes	Distance (km)	km/minute	Corrected Dist. / T (km/min.)	Total Dist. (km)
D	1314-1326	12.00	2.40	0.20	0.20	2.40
	1326-1330	4.00	2.00	0.50	0.30	1.20
	1330-1345	15.00	4.40	0.29	0.33	4.97
	1345-1400	15.00	4.60	0.31	0.37	5.50
	1400-1415	15.00	4.10	0.27	0.29	4.37
	1415-1430	15.00	4.10	0.27	0.28	4.27
	1430-1444	14.00	3.10	0.22	0.26	3.58
	1444-1500	16.00	4.10	0.26	0.25	4.01
	1500-1515	15.00	4.40	0.29	0.26	3.86
	1515-1530	15.00	4.10	0.27	0.27	4.11
	1530-1545	15.00	3.30	0.22	0.26	3.93
	1545-1600	15.00	4.10	0.27	0.26	3.83
	1600-1615	15.00	4.80	0.32	0.27	4.07
	1615-1630	15.00	4.80	0.32	0.30	4.57
	1630-1645	15.00	3.70	0.25	0.30	4.43
	1645-1700	15.00	4.80	0.32	0.30	4.43
	1700-1730	30.00	5.70	0.19	0.25	7.57
	1730-1747	17.00	3.10	0.18	0.23	3.92
	1747-1802	15.00	3.50	0.23	0.20	3.03
	1802-1818	16.00	2.60	0.16	0.19	3.08
	1818-1831	13.00	4.40	0.34	0.24	3.18
	1831-1845	14.00	4.30	0.31	0.27	3.77
	1845-1850	5.00	5.90	1.18	0.61	3.04
	1850-1915	25.00	4.10	0.16	0.55	13.76
	1915-1930	15.00	20.40	1.36	0.90	13.52
	1930-1938	8.00	2.00	0.25	0.59	4.73
	1938-1945	7.00	5.50	0.79	0.80	5.59
	1945-2000	15.00	17.40	1.16	0.73	10.98
					Total Dist. (km)	139.70

Seismic Line #	Time Interval	# Minutes	Distance (km)	km/minute	Corrected Dist. / T (km/min.)	Total Dist. (km)
E	1500-1515	15.00	3.70	0.25	0.25	3.73
	1515-1532	17.00	3.50	0.21	0.23	3.98
	1532-1545	13.00	3.90	0.30	0.25	3.26
	1545-1600	15.00	2.90	0.19	0.23	3.50
	1600-1615	15.00	4.80	0.32	0.27	4.07
	1615-1631	16.00	3.30	0.21	0.24	3.84
	1631-1645	14.00	3.70	0.26	0.26	3.69
	1645-1655	10.00	4.80	0.48	0.32	3.17
	1655-1705	10.00	0.90	0.09	0.28	2.78
	1705-1715	10.00	0.90	0.09	0.22	2.20
	1715-1730	15.00	1.10	0.07	0.08	1.27
	1730-1745	15.00	3.90	0.26	0.14	2.12
	1745-1748	3.00	3.50	1.17	0.50	1.50
					Total Dist. (km)	39.10

Seismic Line #	Time Interval	# Minutes	Distance (km)	km/minute	Corrected Dist. / T (km/min.)	Total Dist. (km)
F	1410-1415	5.00	2.20	0.44	0.44	2.20
	1415-1430	15.00	6.10	0.41	0.43	6.43
	1430-1445	15.00	3.70	0.25	0.36	5.47
	1445-1500	15.00	2.90	0.19	0.28	4.23
	1500-1515	15.00	4.80	0.32	0.25	3.80
	1515-1530	15.00	4.30	0.29	0.27	4.00
	1530-1545	15.00	4.80	0.32	0.31	4.63
	1545-1615	15.00	7.20	0.48	0.36	5.43
	1615-1630	15.00	5.40	0.36	0.39	5.80
	1630-1645	15.00	2.20	0.15	0.33	4.93
	1645-1703	18.00	4.40	0.24	0.25	4.51
	1703-1716	13.00	4.40	0.34	0.24	3.16
	1716-1730	14.00	4.40	0.31	0.30	4.19
	1730-1745	15.00	4.60	0.31	0.32	4.80
	1745-1800	15.00	4.10	0.27	0.30	4.47
					Total Dist. (km)	65.86

Seismic Line #	Time Interval	# Minutes	Distance (km)	km/minute	Corrected Dist. / T (km/min.)	Total Dist. (km)
G	0553-0615	22.00	4.10	0.19	0.19	4.15
	0615-0630	15.00	5.60	0.37	0.25	3.75
	0630-0645	15.00	4.40	0.29	0.28	4.27
	0645-0700	15.00	3.30	0.22	0.30	4.43
	0700-0715	15.00	4.80	0.32	0.28	4.17
	0715-0730	15.00	3.50	0.23	0.26	3.87
	0730-0745	15.00	3.30	0.22	0.26	3.87
	0745-0800	15.00	3.50	0.23	0.23	3.43
	0800-0806	6.00	2.20	0.37	0.27	1.64
	0806-0819	7.00	2.00	0.29	0.30	2.07
	0819-0830	11.00	3.70	0.34	0.33	3.63
	0830-0845	15.00	6.80	0.45	0.36	5.38
	0845-0901	16.00	3.70	0.23	0.34	5.45
	0901-0914	13.00	3.50	0.27	0.32	4.13
	0914-0917	3.00	1.10	0.37	0.29	0.87
	0917-0930	3.00	2.80	0.93	0.52	1.57
	0930-0932	2.00	1.80	0.90	0.73	1.47
	0932-0941	9.00	2.00	0.22	0.69	6.17
	0941-0950	9.00	5.60	0.62	0.58	5.23
	0950-1000	10.00	5.40	0.54	0.46	4.61
	1000-1015	15.00	5.40	0.36	0.51	7.61
	1015-1027	12.00	2.00	0.17	0.36	4.27
	1027-1045	18.00	5.40	0.30	0.28	4.96
	1045-1055	10.00	3.10	0.31	0.26	2.59
					Total Dist. (km)	57.93

Appendix - G Coordinates for Determination of Volume of Holocene Sedime

Seismic Line	Time (hrs)	Latitude DEGREES	Latitude MINUTES	Longitude DEGREES	Longitude MINUTES	x (m)	y (m)	Depth z (m) MODERN
A	0710	21	19.5	91	14.8	233590.43	146693.40	-13.3
	1000	21	11.5	91	14.6	233243.85	131931.80	-15
	0845	21	9.6	91	15.0	233937.00	128425.92	-15
	0900	21	13.0	91	15.0	233937.00	134699.60	-16.66
	1045	21	7.0	91	15.2	234283.57	123628.40	-22.5
	1100	21	6.1	91	16.0	235669.87	121967.72	-26.6
	1115	21	3.0	91	15.0	233937.00	116247.60	-33.3
	1130	21	2.0	91	15.2	234283.57	114402.40	-46.6
	1145	20	59.5	91	16.0	237204.40	109776.51	-62.5
	1200	20	57.6	91	16.0	237204.40	106271.04	-68.3
	1218	20	53.5	91	15.5	236332.33	98706.61	-70.8
	1230	20	52.5	91	16.0	237204.40	96861.63	-75
	1300	20	44.1	91	15.2	235809.08	81363.77	-77.5
	1315	20	42.0	91	15.8	236855.57	77489.30	-79.16
	1320	20	41.0	91	15.7	236681.16	75644.32	-79.16

Seismic Line	Time (hrs)	Latitude DEGREES	Latitude MINUTES	Longitude DEGREES	Longitude MINUTES	x (m)	y (m)	Depth z (m) MODERN
B	1905	21	34.0	90	35.6	165662.05	173448.80	-8.57
	1915	21	33.7	90	34.8	164275.76	172895.24	-8.57
	1930	21	33.8	90	33.0	161156.60	173079.76	-7.5
	1945	21	34.5	90	31.8	159077.16	174371.40	-7.5
	2000	21	34.2	90	30.2	156304.57	173817.84	-6.42
	2015	21	35.0	90	29.0	154225.13	175294.00	-7.5
	2046	21	34.8	90	35.5	165488.77	174924.96	-7.5
	2100	21	35.5	90	35.0	164622.33	176216.60	-7.5
	2115	21	35.5	90	23.0	143827.93	176216.60	-7.5
	2130	21	35.0	90	21.2	140708.77	175294.00	-7.5
	2146	21	35.0	90	19.5	137762.90	175294.00	-7.5

Seismic Line	Time (hrs)	Latitude DEGREES	Latitude MINUTES	Longitude DEGREES	Longitude MINUTES	x (m)	y (m)	Depth z (m) MODERN
C	0920	21	22.0	90	8.0	114369.20	151306.40	-16.66
	0931	21	21.7	90	5.1	112809.62	150752.84	-18.3
	0945	21	19.8	90	5.0	112636.33	147246.96	-20
	1000	21	17.0	90	4.5	111769.90	142080.40	-23.3
	1015	21	15.4	90	4.2	111250.04	139128.08	-27.5
	1030	21	14.2	90	4.0	110903.47	136913.84	-38.33
	1045	21	12.0	90	3.3	109690.46	132854.40	-55
	1100	21	8.5	90	2.8	108824.03	126396.20	-68.3
	1115	21	7.5	90	2.8	108824.03	124551.00	-77.5
	1130	21	6.2	90	2.6	108477.45	122152.24	-82.5
	1145	21	4.1	90	2.0	107437.73	118277.32	-85
	1200	21	2.8	90	1.7	106917.87	115878.56	-86.6

NOTE: Axis Origin 20 N, 89 E

Seismic Line	Time (hrs)	Latitude DEGREES	Latitude MINUTES	Longitude DEGREES	Longitude MINUTES	x (m)	y (m)	Depth z (m) MODERN
D	1314	21	2.6	89	59.0	102239.13	115509.52	-46.6
	1328	21	3.5	89	58.2	100852.84	117170.20	-50.4
	1330	21	3.8	89	57.2	99119.97	117723.76	-51.1
	1345	21	2.9	89	55.0	95307.67	116063.08	-51.8
	1400	21	5.2	89	54.0	93574.80	120307.04	-50.5
	1415	21	5.9	89	51.9	89935.78	121598.68	-50.5
	1430	21	6.5	89	50.2	86989.91	122705.80	-48.4
	1444	21	7.6	89	47.0	81444.73	124735.52	-47.7
	1500	21	8.5	89	44.5	77112.57	126396.20	-47
	1515	21	5.5	89	43.3	75033.13	120860.60	-45.7
	1530	21	9.5	89	41.5	71913.97	128241.40	-45
	1545	21	9.2	89	41.5	71913.97	127687.84	-43.6
	1600	21	9.2	89	39.5	68448.23	127687.84	-43.6
	1615	21	10.1	89	37.0	64116.07	129348.52	-45
	1630	21	12.0	89	36.5	63249.63	132854.40	-50.5
	1645	21	9.5	89	34.5	59783.90	128241.40	-63.4
	1700	21	12.5	89	32.0	55451.73	133777.00	-307
	1730	21	12.7	89	28.5	49386.70	134148.04	-458.8
	1747	21	13.6	89	27.0	46787.40	135806.72	-495
	1802	21	14.0	89	26.0	45054.53	136544.80	-237.3
	1818	21	14.3	89	24.2	41935.37	137098.36	-270
	1831	21	14.5	89	22.0	38123.07	137467.40	-237.3
	1845	21	16.2	89	21.0	36390.20	140604.24	-36.8
	1850	21	14.0	89	19.0	32924.47	136544.80	-30
	1930	21	26.5	89	26.5	45920.97	159609.80	-42.9
	1945	21	27.2	89	27.2	47133.97	160901.44	-79.1
	2000	21	17.2	89	25.6	44361.39	142449.44	-46.4

Seismic Line	Time (hrs)	Latitude DEGREES	Latitude MINUTES	Longitude DEGREES	Longitude MINUTES	x (m)	y (m)	Depth z (m) MODERN
E	1500	21	26.2	89	31.0	53718.87	159056.24	-17
	1515	21	25.0	89	32.5	56318.17	156842.00	-102.9
	1532	21	24.0	89	34.3	59437.33	154996.80	-195
	1545	21	24.0	89	36.5	63249.63	154996.80	-165
	1600	21	23.6	89	38.0	65848.93	154258.72	-90
	1615	21	23.5	89	41.0	71047.53	154074.20	-45
	1631	21	22.2	89	39.8	68968.09	151675.44	-62
	1645	21	23.0	89	37.5	64982.50	153151.60	-150
	1655	21	21.5	89	37.3	64635.93	150383.80	-85.2
	1705	21	21.0	89	37.3	64635.93	149461.20	-78.4
	1715	21	20.0	89	37.0	64116.07	147618.00	-94.1
	1730	21	19.5	89	37.7	65329.07	146693.40	-93.4
	1745	21	17.5	89	37.0	64116.07	143003.00	-95.5
	1748	21	16.0	89	36.5	63249.63	140235.20	-96.1

NOTE: Axis Origin 20 N, 89 E

Seismic Line	Time (hrs)	Latitude DEGREES	Latitude MINUTES	Longitude DEGREES	Longitude MINUTES	x (m)	y (m)	Depth z (m) MODERN
F	1410	21	10.0	89	8.5	14729.37	129164.00	-62
	1415	21	9.5	89	9.0	15595.80	128241.40	-62
	1430	21	7.0	89	11.6	20101.25	123628.40	-63.4
	1445	21	7.2	89	13.3	23047.13	123997.44	-64.7
	1500	21	6.4	89	14.8	25646.43	122521.28	-65.4
	1515	21	6.9	89	17.3	29978.59	123443.88	-67.5
	1530	21	6.2	89	19.6	33964.19	122152.24	-69.5
	1545	21	5.0	89	22.0	38123.07	119938.00	-70.9
	1615	21	5.0	89	26.2	45401.11	119938.00	-64.1
	1630	21	6.5	89	28.2	48866.84	122705.60	-60
	1645	21	7.8	89	29.1	50426.42	125104.56	-42.9
	1703	21	8.5	89	31.5	54585.30	126396.20	-39.5
	1716	21	6.5	89	32.6	56491.45	122705.60	-40.2
	1730	21	6.5	89	35.0	60650.33	122705.60	-40.9
	1745	21	6.0	89	36.3	62903.06	121783.20	-39.5
	1800	21	6.0	89	39.5	68448.23	121783.20	-39.5

Seismic Line	Time (hrs)	Latitude DEGREES	Latitude MINUTES	Longitude DEGREES	Longitude MINUTES	x (m)	y (m)	Depth z (m) MODERN
G	0553	21	31.0	91	26.9	254558.11	167913.20	-15
	0615	21	29.5	91	28.5	257330.70	165145.40	-15
	0630	21	31.5	91	31.5	262529.30	168835.80	-16.4
	0645	21	27.0	91	33.2	265475.17	160532.40	-18.4
	0700	21	25.6	91	34.2	267208.04	157949.12	-19.7
	0715	21	27.5	91	36.5	271193.63	161455.00	-19.7
	0730	21	28.0	91	38.4	274486.08	162377.60	-20.5
	0745	21	28.6	91	40.0	277258.67	163484.72	-20.5
	0800	21	27.9	91	42.2	281070.97	162193.08	-19.7
	0806	21	27.5	91	43.0	282457.27	161455.00	-19.7
	0819	21	29.5	91	43.0	282457.27	165145.40	-19.7
	0830	21	29.8	91	44.5	285056.57	165698.96	-19.1
	0845	21	29.8	91	47.0	289388.73	165698.96	-25.2
	0901	21	34.2	91	47.5	290255.17	173817.84	-36.8
	0914	21	32.5	91	49.0	292854.47	170681.00	-23.2
	0917	21	32.0	91	49.3	293374.33	169758.40	-23.2
	0930	21	31.5	91	48.0	291121.60	168835.80	-34.7
	0932	21	32.0	91	47.5	290255.17	169758.40	-34.7
	0941	21	32.6	91	47.3	289908.59	170865.52	-34.7
	0950	21	35.6	91	46.5	288522.30	176401.12	-34.7
	1000	21	38.5	91	46.2	288002.44	181752.20	-26.6
	1015	21	48.0	91	46.0	287655.87	199281.60	-32.7
	1027	21	42.0	91	46.5	288522.30	188210.40	-27.9
	1045	21	41.0	91	43.7	283670.27	186365.20	-15
	1055	21	41.6	91	41.7	280204.54	187472.32	-22.5

NOTE: Axis Origin 20 N, 89 E

Misc Pts:

Boundaries

	Latitude DEGREES	Latitude MINUTES	Longitude DEGREES	Longitude MINUTES	x (m)	y (m)	Depth z (m) MODERN
BATHYMETRY	21	10.5	92	2.3	315814.95	130086.60	-10
OF BAY OF BENGAL	21	8.3	91	57.5	307583.83	125934.90	-20
	21	16.0	92	0.8	313215.65	140235.20	-10
	21	8.5	91	53.0	299785.93	122705.80	-30
	21	3.0	91	44.0	284190.13	116247.60	-50
	21	24.0	91	55.0	303251.67	154998.80	-10
	21	19.5	91	54.5	302385.23	146693.40	-10
	21	14.5	91	48.0	291121.60	137467.40	-20
	21	28.5	91	50.5	295453.77	163300.20	-20
	21	22.5	91	48.5	291988.03	152229.00	-20
	21	13.8	91	45.0	285923.00	136083.50	-30
	21	20.0	91	44.0	284190.13	147616.00	-20
	21	30.0	91	46.5	288522.30	166068.00	-20
	21	39.5	91	46.0	287655.87	183597.40	-20
	21	48.0	91	44.5	285056.57	199281.60	-10
	21	22.0	91	38.0	273792.93	151306.40	-20
	21	8.5	91	39.0	275525.80	122705.80	-50
	21	0.0	91	28.5	257330.70	110712.00	-50
	21	13.0	91	35.0	268594.33	134699.60	-30
	21	5.5	91	21.5	245200.63	120860.60	-30
	21	14.0	91	31.0	261662.87	136544.80	-20
	21	1.0	91	13.0	230471.27	112557.20	-50
	21	7.0	91	15.0	233937.00	123628.40	-20
	21	7.0	91	3.0	213142.60	123628.40	-20
	21	4.5	91	3.0	213142.60	119015.40	-30
	21	2.5	91	3.0	213142.60	115325.00	-50
	21	41.5	91	43.0	282457.27	187287.80	-10
	21	43.5	91	45.5	286789.43	190978.20	-10
	21	50.5	91	45.5	286789.43	203894.60	-10
	21	44.5	91	44.0	284190.13	192823.40	-10
	21	52.0	91	46.5	288522.30	206662.40	-10
	21	55.0	91	50.5	295453.77	212198.00	-10
	21	56.0	91	51.0	296320.20	214043.20	-10
	21	4.0	91	50.0	294587.33	118092.80	-10
	21	59.0	91	48.5	291988.03	219578.80	-10
	21	58.5	91	45.5	286789.43	218656.20	-10
	21	19.5	91	9.0	223539.80	146693.40	-10
	21	28.5	91	17.0	237402.73	159609.80	-10
	21	19.0	90	57.5	203611.83	145770.80	-10
	21	4.5	90	39.5	172420.23	119015.40	-50
	21	6.5	90	39.5	172420.23	122705.80	-30
	21	9.5	90	39.5	172420.23	128241.40	-20
	21	15.5	90	39.5	172420.23	139312.60	-10
	21	7.0	90	18.5	136030.03	123628.40	-50
	21	10.5	90	18.5	136030.03	130086.60	-30
	21	14.0	90	18.5	136030.03	136544.80	-20
	21	20.0	90	18.5	136030.03	147616.00	-10
	21	40.0	91	24.5	250399.23	184520.00	-10
	21	54.5	91	32.0	263395.73	211275.40	-10
	22	13.0	91	46.0	285697.07	245440.42	-10
	22	18.0	91	42.5	279673.33	250976.67	-10

NOTE: Axis Origin 20 N, 89 E

Latitude DEGREES	Latitude MINUTES	Longitude DEGREES	Longitude MINUTES	x (m)	y (m)	Depth z (m) MODERN
22	24.0	91	43.5	281394.40	265740.00	-10
22	24.5	91	35.0	266765.33	266662.71	-5
22	18.5	91	34.0	265044.27	255590.21	-5
22	15.5	91	35.5	267625.87	250053.96	-5
22	15.5	91	31.5	260741.60	250053.96	-5
22	15.5	91	25.0	249554.67	250053.96	-5
22	21.5	91	21.5	243530.93	261126.46	-5
22	13.5	91	19.5	240088.80	246363.13	-5
22	12.0	91	21.0	242670.40	243595.00	-5
22	7.0	91	18.0	237507.20	234367.92	-5
22	10.0	91	16.5	234925.60	239904.17	-5
22	7.0	91	12.0	227180.80	234367.92	-5
22	1.0	91	6.5	217714.93	223295.42	-5
21	55.0	91	3.0	213142.60	212198.00	-5
21	52.0	90	59.5	207077.57	206662.40	-5
21	52.0	90	55.5	200146.10	206662.40	-5
21	42.5	90	58.5	205344.70	189133.00	-5
21	51.0	90	50.5	191481.77	204817.20	-5
21	48.0	90	53.0	195813.93	199281.60	-5
21	34.0	90	53.0	195813.93	173448.80	-5
21	46.0	90	55.0	199279.67	195591.20	-5
21	43.0	90	56.5	201878.97	190055.60	-5
21	44.5	90	52.5	194947.50	192823.40	-5
21	42.5	90	46.5	184550.30	189133.00	-5
21	35.5	90	46.0	183683.87	176216.60	-5
21	38.0	90	43.5	179351.70	180829.60	-5
21	44.0	90	40.5	174153.10	191900.80	-5
21	39.0	90	40.5	174153.10	182674.80	-5
21	36.0	90	37.0	168088.07	177139.20	-5
21	28.5	90	33.5	162023.03	163300.20	-5
21	38.0	90	28.5	153358.70	180829.60	-5
21	39.0	90	26.0	149026.53	182674.80	-5
21	29.5	90	21.5	141228.63	165145.40	-5
21	11.5	90	2.5	108304.17	131931.80	-50
21	14.0	90	2.5	108304.17	136544.80	-30
21	18.0	90	2.5	108304.17	143925.60	-20
21	23.0	90	2.5	108304.17	153151.60	-10
21	33.0	90	11.5	123899.97	171603.60	-5
21	37.5	90	1.5	106571.30	179907.00	-5
21	14.0	89	50.5	87509.77	136544.80	-50
21	16.5	89	50.5	87509.77	141157.80	-30
21	20.0	89	50.5	87509.77	147616.00	-20
21	28.0	89	50.5	87509.77	162377.60	-10
21	39.5	89	50.5	87509.77	183597.40	-5
21	5.0	89	13.0	22527.27	119938.00	-500
21	6.5	89	13.0	22527.27	122705.80	-200
21	7.5	89	13.0	22527.27	124551.00	-100
21	9.5	89	13.0	22527.27	128241.40	-50
21	11.5	89	13.0	22527.27	131931.80	-30
21	13.5	89	13.0	22527.27	135622.20	-20
21	19.0	89	13.0	22527.27	145770.80	-10
21	1.0	89	16.5	28592.30	112557.20	-500

NOTE: Axis Origin 20 N, 89 E

Latitude MINUTES	Longitude DEGREES	Longitude MINUTES	x(m)	x (m)	y (m)	Depth z (m) MODERN	
	21	31.5	89	5.0	8664.33	166835.80	-5
	21	27.0	89	8.0	13862.93	160532.40	-5
	21	33.0	89	9.5	16462.23	171603.60	-5
	21	34.0	89	10.0	17328.67	173448.80	-10
	21	34.0	89	12.0	20794.40	173448.80	-10
	21	29.5	89	11.0	19061.53	165145.40	-10
	21	13.5	89	17.5	30325.17	135622.20	-200
	21	14.0	89	17.5	30325.17	136544.80	-50
	21	15.0	89	17.5	30325.17	138390.00	-30
	21	16.0	89	17.5	30325.17	140235.20	-20
	21	19.0	89	17.5	30325.17	145770.80	-10
	21	59.0	89	25.0	43321.67	219578.80	-100
	21	3.0	89	20.5	35523.77	116247.60	-200
	21	5.0	89	25.0	43321.67	119938.00	-500
	21	4.5	89	24.0	41588.80	119015.40	-100
	21	9.5	89	24.0	41588.80	128241.40	-500
	21	13.5	89	24.0	41588.80	135622.20	-200
	21	14.0	89	24.0	41588.80	136544.80	-100
	21	29.0	89	39.5	68448.23	164222.80	-10
	21	39.0	89	43.5	75379.70	182674.80	-5
	21	24.5	89	45.0	77979.00	155919.40	-20
	21	20.5	89	41.5	71913.97	148538.60	-30
	21	17.0	89	39.5	68448.23	142080.40	-50

	Latitude DEGREES	Latitude MINUTES	Longitude DEGREES	Longitude MINUTES	x (m)	y (m)	Depth z (m) MODERN
COORDINATES FOR	21	7.5	92	5.0	320580.33	124551.00	0
MODERN COAST	21	24.5	91	58.0	308450.27	155919.40	0
	21	42.5	91	49.5	293720.90	189133.00	0
	21	8.5	91	49.0	292854.47	126396.20	0
	22	26.5	91	42.0	278812.80	270353.54	0
	22	27.5	91	36.0	268486.40	272198.96	0
	22	23.5	91	21.5	243530.93	264817.29	0
	22	19.0	91	31.5	260741.60	256512.92	0
	22	16.0	91	19.0	239228.27	250976.67	0
	22	2.5	91	7.5	219436.00	226063.54	0
	21	53.0	90	58.0	204478.27	208507.60	0
	21	50.5	90	49.5	189748.90	203894.60	0
	21	46.0	90	47.0	185416.73	195591.20	0
	21	47.0	90	39.0	171553.80	197436.40	0
	21	43.5	90	28.5	153358.70	190978.20	0
	21	43.0	90	17.5	134297.17	190055.60	0
	21	45.0	90	9.5	120434.23	193746.00	0
	21	50.5	89	57.0	98773.40	203894.60	0
	21	46.5	89	48.0	83177.60	196513.80	0
	21	46.5	89	43.5	75379.70	196513.80	0
	21	43.0	89	39.0	67581.80	190055.60	0
	21	46.0	89	29.0	50253.13	195591.20	0
	21	43.0	89	24.0	41588.80	190055.60	0
	21	44.5	89	18.5	32058.03	192823.40	0
	21	38.5	89	16.0	27725.87	181752.20	0
	21	37.0	89	6.0	10397.20	178984.40	0

NOTE: Axis Origin 20 N, 89 E

	Latitude DEGREES	Latitude MINUTES	Longitude DEGREES	Longitude MINUTES	x (m)	y (m)	Depth z (m) MODERN
WESTERN	21	31.5	89	3.5	6065.03	168835.80	-5
BOUNDARY AT	21	23.0	89	4.5	7797.90	153151.60	-5
SWATCH OF NO	21	14.5	89	7.0	12130.07	137467.40	-10
GROUND	21	12.0	89	7.5	12998.50	132854.40	-20
	21	9.5	89	8.0	13862.93	128241.40	-30
	21	8.0	89	9.5	16462.23	125473.60	-50
	21	6.0	89	11.0	19061.53	121783.20	-100
	21	5.0	89	11.5	19927.97	119938.00	-200
	21	3.5	89	12.5	21660.83	117170.20	-500
	20	59.0	89	16.0	27906.40	108854.02	-500
	20	58.0	89	18.0	31394.70	107009.03	-200

	Latitude DEGREES	Latitude MINUTES	Longitude DEGREES	Longitude MINUTES	x (m)	y (m)	Depth z (m) MODERN
WESTERN INLAND	22	31.0	89	8.5	11186.93	278657.92	-16
BOUNDARY	22	14.0	89	5.0	8805.33	247285.83	-16
TO SWATCH OF NO	21	58.0	89	5.0	8664.33	217733.60	-16
GROUND	21	45.0	89	4.5	7797.90	193746.00	-16

	Latitude DEGREES	Latitude MINUTES	Longitude DEGREES	Longitude MINUTES	x (m)	y (m)	Depth z (m) MODERN
NORTH EAST-WEST	22	36.0	91	37.0	270207.47	287885.00	-16
BOUNDARY	22	45.0	91	20.0	240949.33	304493.75	-16
THROUGH KHULNA	22	48.0	91	0.0	206528.00	310030.00	-16
CITY	22	50.0	90	44.0	178990.93	313720.83	-16
	22	53.0	90	26.0	148011.73	319257.08	-16
	22	52.0	90	6.0	113590.40	317411.67	-16
	22	53.0	89	32.0	55074.13	319257.08	-16
	22	48.0	89	13.0	22373.87	310030.00	-16

* coordinate system is based on the distance in meters between degrees of latitude and longitude with an arbitrary axis origin of 20 N, 80E.
z = depth below sea level (m).

NOTE: Axis Origin 20 N, 89 E

References

Alexander, C.R., Nittrouer, C.A., DeMaster, D.J. (1986). High-Resolution Seismic Stratigraphy and its Sedimentological Interpretation of the Amazon Continental Shelf. Continental Shelf Research, 6, No. 1/2: 337-357.

Alexander, C.R., DeMaster, D.J. and Nittrouer, C.A. (1991). Sediment Accumulation in a Modern Epicontinental-shelf Setting: The Yellow Sea. Marine Geology, 98: 51-72.

Asquith, D.O. (1970). Depositional Topography and Major Marine Environments, Late Cretaceous, Wyoming. The America Association of Petroleum Geologists, 54, No. 7: 1184-1224.

Barua, D.K. (1990). Suspended Sediment Movement in the Estuary of the Ganges-Brahmaputra-Meghna River System. Marine Geology, 9 : 243-253.

Barua, D.K., Kuehl, S.A., Miller, R.L. and Moore W.S. (1994). Suspended Sediment Distribution and Residual Transport in the Coastal Ocean off of the

Ganges-Brahmaputra River Mouth. Marine Geology, 120:41-61.

Coleman, J.M. (1969). Brahmaputra River: Channel Processes and Sedimentation. Sedimentary Geology, 3, No. 2/3 : 129-239.

Curray, J.R. and Moore, D.G. (1971). Growth of the Bengal Deep-Sea Fan and Denudation in the Himalayas. Geological Society of America Bulletin, 82 : 563- 572.

Curray, J.R. and Moore, D.G. (1974). *Sedimentary and Tectonic Processes in the Bengal Deep-Sea Fan and Geosyncline.* in: Continental Margins, C.A. Burk and C.L. Drake (Editors), New York, Springer-Verlag: 617-627.

Curray, J.R., Emmel, F.J., Moore, D.G. and Rait, R.W. (1982). *Structure, Tectonics and Geological History of the Northeastern Indian Ocean.* in: A.E. Nairn,and F.G. Stehli, (Editors). The Ocean Basins and Margins. Vol. 6 : New York, Plenum Press : 399-450.

Cutshall, N.H., Larsen, I.L. and Olsen, C.R. (1983). Direct Analysis of ^{210}Pb in

Sediment Samples: Self-Absorption Correction. Nuclear Instruments and Methods, 206: 309-312.

DeMaster, D.J., Kuehl, S.A., Nittrouer, C.A. (1986). Effects of Suspended Sediment on Geochemical Processes Near the Mouth of the Amazon River: Examination of Biological Silica Uptake and the Fate of Particle Reactive Elements. Continental Shelf Research, 6, No. 1/2 : 107-125.

Dukat, D.A. and Kuehl, S.A. (in press). Investigations of Non-Steady-State ^{210}Pb flux and the Use of $^{228}Ra/^{226}Ra$ as a Geochronometer on the Amazon Continental Shelf. Marine Geology.

Emmel, F.J. and Curray, J.R. (1985). *Bengal Fan, Indian Ocean*. in: A.H. Bouma, W.R Normark, and N.E. Barnes (Editors), Submarine Fans and Related Turbidite Systems: New York, Springer Verlag, : 107-112.

Figueiredo, A.G., Jr. and Nittrouer, C.A. (in press). New Insights to High-Resolution Stratigraphy on the Amazon Shelf. Marine Geology.

Gibbs, R.J. (1967). The Geochemistry of the Amazon River System: Part I. The Factors that Control the Salinity and the Composition and Concentration of the Suspended Solids. Geological Society of America Bulletin, 78: 1203-1232.

Goldberg, E.D. and Koide, M. (1962). Geochronological Studies of Deep Sea Sediments by the Ionium/Thorium Method. Geochimica et Cosmochimica Acta, 26 : 417-450.

Hariu, T. (1988). The Nature of Sedimentation Seaward of the Ganges River System. Master's Thesis, University of South Carolina-Columbia.

Klootwijk, C.T., Gee, J.S., Peirce, J.W. and Smith, G.M. (1992). Neogene Evolution of the Himalayan-Tibetan Region: Constraints from ODP Site 758, Northern Ninetyeast Ridge; Bearing on Climatic Change. Palaeogeography, Palaeoclimatology, Palaeoecology, 95: 95-110.

Koide, M., Soutar, A. and Goldberg, E.D. (1973). Marine Geochronology With ^{210}Pb. Earth Science Letters, 14, No. 3: 442-446.

Kuehl, S.A., DeMaster, D.J. and Nittrouer, C.A. (1986). Nature of Sediment Accumulation on the Amazon Continental Shelf. Continental Shelf Research, 6: 209-225.

Kuehl, S.A., Nittrouer, C.A. and DeMaster, D.J. (1988). Microfabric Study of Fine-grained Sediments: Observations From the Amazon Subaqueous Delta. Journal of Sedimentary Petrology, 58, No. 1: 12-23.

Kuehl, S.A., Hariu, T.M. and Moore, W.S. (1989). Shelf Sedimentation off the Ganges-Brahmaputra River System: Evidence for Sediment Bypassing to the Bengal Fan. Geology, 17: 1132-1135.

Leithold, E. L. (1994). Stratigraphical Architecture at the Muddy Margin of the Cretaceous Western Interior Seaway, Southern Utah. Sedimentology, 41: 521-542.

Leithold, E. L. (1993). Preservation of Laminated Shale in Ancient Clinoforms: Comparison to Modern Subaqueous Deltas. Geology, 2 : 359-362.

McKee, B.A., DeMaster, D.J. and Nittrouer, C.A. (1986). Temporal Variability in the Partitioning of Thorium Between Dissolved and Particulate Phases on the Amazon Shelf: Implications for the Scavenging of Particle-Reactive Species. Continental Shelf Research, 6, No. 1/2: 87-106.

Milliman, J.D. (1979). Morphology and Structure of Amazon Continental Margin. The American Association of Petroleum Geologists Bulletin, 63, No. 6: 934-950.

Milliman, J.D. and Syvitski, J.P.M. (1992). Geomorphic/Tectonic Control of Sediment Discharge to the Ocean: The Importance of Small Mountainous Rivers. The Journal of Geology, 100: 525-544.

Morgan, J.P. and McIntire, W.G. (1959). Quaternary Geology of the Bengal Basin, East Pakistan and India. Bulletin of the Geological Society of America, 70: 319-342.

Murty, V.S.N., Sarma, Y.V.B., Rao, D.P. and Murty, C.S. (1992). Water Characteristics, Mixing and Circulation in the Bay of Bengal during Southwest Monsoon. Journal of Marine Research, 50 : 207-228.

Nittrouer, C.A., Sternberg, R.W., Carpenter, R. and Bennett, J.T. (1979). The Use of Pb-210 Geochronology as a Sedimentological Tool: Application to the Washington Continental Shelf. Marine Geology, 31: 297-316.

Nittrouer, C.A., Kuehl, S.A., DeMaster, D.J. and Kowsmann, R.O. (1986). The Deltaic Nature of Amazon Shelf Sedimentation. Geological Society of American Bulletin, 97: 444-458.

Nittrouer, C.A., Kuehl, S.A., Sternber, R.W., Figueiredo, A.G., Jr., and Faria, L.E.C. (In press). An Introduction to the Geological Significance of Sediment Transport and Accumulation on the Amazon Continental Shelf. Marine Geology.

Polach, H.A. and Stipp, J.J. (1967). Improved Synthesis Technique for Methane and Benzene Radiocarbon Dating. International Journal of Applied Radiation and Isotopes, 18: 359-364.

Prior, D.B., Yang, Z.S., Bornhold, B.D., Geller, G.H.,Lin, Z.H., Wiseman, W.J.,

Jr., Wright, L.D. and Lin, T.C. (1986). The Subaqueous Delta of the Modern Huanghe (Yellow River). Geo-Marine Letters, 6: 67-75.

Rao, V.P. (1991). Clay Mineral Distribution in the Continental Shelf Sediments from Krishna to Ganges River Mouth, East Coast of India. Indian Journal of Marine Sciences. 20: 7-12.

Rao, V.P., Reddy, N.P. and Rao, C.M. (1988). Clay Mineralogy Distribution in the Shelf Sediments off the Coast of the Northern Part of the East Coast of India. Continental Shelf Research, 8: 145-151.

Rao, M. S. (1964). Some Aspects of Continental Shelf Sediments off the East Coast of India. Marine Geology, 1:5-87

Sarin, M.M., Krishnaswami, S., Dili, K., Somayajulu, B.L.K. and Moore, W.S. (1989). Major Ion Chemistry of the Ganges-Brahmaputra River System: Weathering Processes and Fluxes to the Bay of Bengal. Geochemica et Cosmochimica Acta, 53: 997-1009.

Segall, M.P. and Kuehl, S.A. (1992). Sedimentary Processes on the Bengal Shelf as Revealed by Clay-size Mineralogy. Continental Shelf Research, 12, No. 4: 517-541.

Sommerfield, C.K., Nitrrouer, C.A. and Figueiredo, A.G. (in press). Stratigraphic Evidence of Changes in Amazon Shelf Sedimentation During the Late Holocene. Marine Geology.

Suryanarayana, A., Murty, C.S. and Rao, D.P. (1992). Characteristics of Coastal Waters of the Western Bay of Bengal during Different Monsoon Seasons. Australian Jouranal of Freshwater Ressearch, 43, 1517-33.

Umitsu, M. (1987). Late Quaternary Sedimentary Environment and Landform Evolution in the Bengal Lowland. Geographical Review of Japan, 60, No. 2, 164-178.

Umitsu, M. (1990). Late Quaternary Environments and Landforms in the Ganges Delta. Sedimentary Geology, 83: 177-186.

Wright, L.D. and Coleman, J.M. (1973). Variations in Morphology of Major Deltas as Functions of Ocean Wave and River Discharge Regimes. American Association of Petroleum Geologists Bulletin, 57, No. 2, 370-398.

Wright, L.D. and Coleman, J.M. (1974). Mississippi River Mouth Processes: Effluent Dynamics and Morphologic Development. Journal of Geology, 82: 751-778.

Wyrtki, K. (1973). *Physical Oceanography of the Indian Ocean.* in: B. Zeitzschel (Editor), Ecology Studies 3b, The Biology of the Indian Ocean. Springer Verlag. ppp. 18-36.